UNIVERSIDADE NOVA DE LISBOA

Faculdade de Ciências e Tecnologia

Departamento de Física

A first analysis of the atmospheric measurements from TANSO/GOSAT

Bárbara Sofia Santos Teixeira

Dissertação apresentada na Faculdade de Ciências e Tecnologia da Universidade Nova de Lisboa para obtenção do grau em Mestre em Engenharia Física

(a presente dissertação foi preparada no âmbito do Protocolo Sócrates/ERASMUS existente entre a FCT-UNL e a Université Libre de Bruxelles)

Orientador: Prof. Doutor Pierre-François Coheur (ULB)

Lisboa
2010

Agradecimentos

Começo por agradecer ao Professor Pierre-François Coheur, da Université Libre de Bruxelles, por ter coordenado este trabalho mas também pelo seu apoio e conhecimentos transmitidos.

Agradeço também a todas as pessoas pertencentes ao serviço de Chimie quantique et photophysique da Université Libre de Bruxelles.

Aos Professores José Paulo dos Santos e Gregoire Bonfait, da FCT-UNL, pela ajuda prestada durante todo o processo relativo à mobilidade ERASMUS, no âmbito da qual este trabalho foi efectuado.

Aos meus colegas de trabalho na ULB Ariane Razavi, Stéphane Vranckx, Simon Chefdeville, Yasmina R'Honi, Lieven Clarisse e Jean-Lionel Lacour.

Aos meus colegas e amigos da FCT-UNL Daniel Martins e Joaquim Conde, bem como a todos os restantes colegas do MIEF.

À minha família mais próxima, mãe e avó, aos meus amigos e ao Ariën, pelo incondicional apoio ao longo de todo este percurso.

Um último agradecimento, fica reservado ao meu falecido avô, que certamente gostaria de estar presente neste momento.

Resumo

Este trabalho analisa os espectros atmosféricos registados pelo instrumento TANSO-FTS a bordo da plataforma GOSAT, com o objectivo de avaliar a utilidade dessas medidas para as aplicações químicas, em especial para monitorizar compostos de azoto reactivo na baixa atmosfera.

Como uma missão dedicada para o clima, GOSAT tem uma série de vantagens sobre outras sondas, como a alta resolução espectral e uma extensa cobertura das regiões espectrais do infravermelho térmico e de ondas curtas de infravermelho. Na primeira parte do nosso trabalho, determinamos, através da realização de um conjunto de cálculos de transferência radiativa, as bandas moleculares que compõem o espectro TANSO-FTS nas diferentes regiões do espectro, e as espécies que poderiam potencialmente ser detectados em condição de alta poluição. Mostramos em particular, que N_2O e NH_3 têm assinaturas de absorção na banda SWIR número 2, que poderia ser utilizada - a prossecução do trabalho é necessária para uma avaliação definitiva - para melhorar a monitorização da fonte.

Na segunda parte deste trabalho, concentramo-nos nas medições de TANSO-FTS no infravermelho térmico e proporcionar um estudo comparativo com as medidas de radiância validadas e bem estudadas realizada pelo instrumento IASI a bordo da plataforma MetOp. Através de uma inter-comparação sobre os oceanos com rigorosos critérios de co-localização e congruência temporal, mostramos que as radiâncias medidas pelo TANSO-FTS a serem 2 K superiores em relação ao IASI para medições durante o dia, sendo que para a noite, radiâncias do TANSO-FTS a serem 0,7 K inferiores em relação ao IASI. Nós também achamos que a *line shape* teórica não está perfeitamente adaptada para reproduzir as medições. Essas são questões que precisam de atenção para uma análise mais sofisticada com GOSAT. Ainda assim, baseando-se num método simples de indexação de radiância e cálculos de diferença de temperatura de brilho, podem comprovar que o TANSO-FTS tem capacidades de detecção considerável de NH_3, aparentemente, superiores aos do IASI. O instrumento é indicado para fazer a detecção inequívoca de *hotspots* numa base diária e permitir capturar as variações sazonais em todos os meses, inclusive no inverno, quando a concentração de NH_3 é mais fraca.

Abstract

This work examines the atmospheric spectra recorded by the TANSO-FTS instrument onboard the GOSAT platform, with the aim of assessing the usefulness of these measurements for chemistry applications, and in particular for monitoring reactive nitrogen compounds in the low atmosphere.

As a dedicated mission for climate, GOSAT has a series of advantages over other sounders, such as high spectral resolution and extensive coverage of thermal infrared and shortwave infrared spectral regions. In the first part of our work, we determine, by performing a set of radiative transfer calculations, the molecular bands which compose the TANSO-FTS spectra in the different spectral regions, and the species which could potentially be detected under high pollution condition. We show in particular that N_2O and NH_3 have absorption signatures in the SWIR band number 2, which could possibly be used – further work is needed for a definitive assessment – to improve on source monitoring.

In the second part of this work, we concentrate on the thermal infrared measurements of TANSO-FTS and provide a comparative study with the validated and well-studied radiance measurements performed by the IASI instrument onboard MetOP. Through an inter-comparison over the oceans with strict criteria of co-localization and temporal matching, we show the TANSO-FTS radiances to be biased high by 2 K as compared to IASI for day-time measurements, while for night-time TANSO-FTS radiances to be biased low by 0.7 K as compared to IASI. We also find that the theoretical line shape is not perfectly adapted for reproducing the measurements. These are issues that need attention for more sophisticated analysis with GOSAT. Still, relying on a simple radiance indexing method and brightness temperature difference calculations, we were able show that the TANSO-FTS has considerable detection capabilities of NH_3, apparently by far superior to those of IASI. The instrument is shown to make unambiguous detection of hotspots on a daily basis and to enable capturing seasonal variations in all months, including in winter when the NH_3 concentration are weakest.

Table of contents

Agradecimentos 2

Resumo 3

Abstract 4

Introduction 11

1. TANSO/GOSAT and IASI/MetOp satellites sounders 14
   - 1.1 GOSAT science objectives 14
   - 1.2 GOSAT orbit and TANSO instrument 16
   - 1.3 "Atmospheric Composition and Chemistry-Climate interactions with GOSAT": Background – from IASI and objectives 21

2. Atmospheric radiative transfer (non-scattering atmosphere) applied to GOSAT 26
   - 2.1 General formulation 26
   - 2.2 Simplification for the TIR 30
   - 2.3 Formulation for the SWIR; reflectivity of surfaces 31

3. Objective of this research 34

4. Results and discussions 35
   - 4.1 TANSO measurements in the SWIR 35
     - 4.1.1. Overview per band 35
   - 4.2 TANSO measurements in the TIR 39
     - 4.2.1. Overview 39
     - 4.2.2. Radiometric cross-calibration between TANSO-FTS and IASI 41
     - 4.2.3. Spectral calibrations and Instrument response function 46
   - 4.3 On the potential use of TANSO/GOSAT for monitoring the nitrogen cycle 48
     - 4.3.1. The perturbed cycle of reactive nitrogen 48
     - 4.3.2. Measuring NH_3 from GOSAT: method 49

4.3.3. Global NH_3 and comparison with IASI 51
4.3.4. NH_3 above India: seasonal variations and comparison with IASI 54

5. Conclusions and perspectives 56

6. References 58

Index of figures

Fig. 1 – Role sharing in the GOSAT project. (http://www.gosat.nies.go.jp/) 14

Fig. 2 – Overview of GOSAT in orbit. (http://www.gosat.nies.go.jp/) 15

Fig. 3 – Illustration of a sun-synchronous orbit. Figure courtesy of the National Space Agency of Japan (NASDA) 16

Fig. 4 – GOSAT observation and orbits. (http://www.gosat.nies.go.jp/) 16

Fig. 5 – Radiance observation by TANSO in the short-wave and visible (left) using reflected/scattered solar radiation and in the thermal infrared (right). (http://www.gosat.nies.go.jp/) 17

Fig. 6 – Diagram of a Michelson interferogram. 18

Fig. 7 - Example of a local day-time GOSAT spectrum in the four different spectral bands, from the TIR to the visible. Note: the TIR band was multiplied by a factor or 30 for clarity. 20

Fig. 8 – MetOp and IASI (http://www.esa.int/) 21

Fig. 9 – IASI observation mode. (http://smsc.cnes.fr/IASI/) 22

Fig. 10 – IASI radiometric noise over three spectral bands, in radiance units (black curve) and equivalent delta temperature (blue curve) (Clerbaux *et al*, 2009). 24

Fig. 11 – Example of an IASI spectrum in normalized radiance (top) and with individual molecular contributions highlighted (three following panels), in descending order of importance. (Clerbaux *et al*, 2009) 25

Fig. 12 – Illustration of blackbody curves at 288 K and 6000 K. Note the logarithmic scale of the black-body spectral radiance. 27

Fig. 13 – Illustration of the solid angle definition. 27

Fig. 14 – Example of surfaces' reflectivity. (Petty, 2006) 31

Fig. 15 - Specular reflection. (Petty, 2006) 32

Fig. 16 - Lambertian reflection. 32

Fig. 17 – Individual molecular contributions highlighted for visible band; above Pacific Ocean.37

Fig. 18 – Individual molecular contributions highlighted for SWIR 2 band; above Pacific Ocean. 38

Fig. 19 - Unknown signature present in every TANSO-FTS spectrum. 38

Fig. 20 – Individual molecular contributions highlighted for SWIR 3 band; above Pacific Ocean. 39

Fig. 21 – Individual molecular contributions highlighted for TIR band; above Pacific Ocean. ..40

Fig. 22 – Night-time spectrum for the thermal infrared range above sea. Left panel: good agreement between TANSO-FTS (blue line) and IASI (red line). Right panel: bad agreement between both satellites. 43

Fig. 23 – Left: histogram of brightness temperature differences for IASI and TANSO-FTS spectra occurred during day-time data. Right: same for night-time data (note: no time filter was applied). 44

Fig. 24 - Relation between the brightness temperatures measured by both satellites. 45

Fig. 25 – Instrumental line shapes for the TANSO-FTS TIR band, provided there is no misalignment in the spectrometer. 46

Fig. 26 – Spectral fitting of TANSO-FTS in a narrow portion of the TIR band. 47

Fig. 27 – Nitrogen Cascade. (Galloway & Aber, 2003) 49

Fig. 28 - Block diagram. 50

Fig. 29 - NH_3 distribution obtained by TANSO-FTS in 3 days (12th, 13th and 14th of March 2010). 52

Fig. 30 - NH_3 global distribution obtained by IASI (12^{th}, 13^{th} and 14^{th} of March 2010). 53

Fig. 31 - NH_3 seasonal variation obtained by IASI: (a) April 2009, (b) July 2009, (c) October 2009, (d) January 2010. 54

Fig. 32 - NH_3 seasonal variation obtained by GOSAT: (a) April 2010, (b) July 2009, (c) October 2009, (d) January 2010. 55

Index of tables

Table 1 - Characteristics of the TANSO-FTS instrument. 18

Table 2 – Characteristics of the TANSO-CAI instrument. (GOSAT, 2009) 20

Table 3 – Characteristics of IASI. (Clerbaux et al, 2009) 23

Table 4 – Parameters used to simulate the molecules' profiles. 36

Table 5 - List of some molecules absorbing in the TIR band of TANSO-FTS 41

Table 6 – Clear windows used for the cross-calibration. 42

Table 7 - Statistical values obtained for both set of data. 44

Table 8 - Parameters used to fit the spectrum. 47

Table 9 - Vibration modes for NH_3; source: HITRAN website. 51

Table 10 – Channels used to calculate the brightness temperature difference with TANSO-FTS and IASI. 51

Introduction

Earth's atmosphere has been dealing with several chemical changes during the years which are reflected in the global environment through some phenomena that can destroy the ozone layer or lead to a global warming.

These changes in the global environment can be due to natural factors that have been happening through years such as variations in the solar flux or even changes in Earth's orbit around Sun since this influence the quantity of energy which is reflected and absorbed (Svensmark & Friis-Christensen, 1997). However, the role played by human in factors that may change global environment has become more important through time. These factors are related with industrial and agricultural activities, in order to give an answer to growing population and an exigent society. They result in the emission of for example greenhouse gases to the atmosphere, or as well of fine particles – the aerosols. There is still another factor that may change the global environment: the land use evolution. Through replacing forest by arable lands or asphalt, Man is modifying the Earth's surface and its way of reflecting the sunlight and release the heat, which may lead to a temperature rise. Due to all these reasons, it became more important to monitor how atmosphere is changing.

With the advance of the technology to probe the atmosphere from the space (remote sensing) as well as the theoretical models of atmospheric radiative transfer, it has been possible to better understand and know which chemical compounds and processes are responsible for global environmental issues. Combining the global observations to chemistry models makes it possible to identify and quantify the sources of these emissions, allowing not only a better knowledge about this subject but also a step forward in science. There are several space missions with this field of study as their main purpose.

This works reports on a first analysis of the atmospheric measurements made by the TANSO instrument onboard GOSAT satellite, which is a dedicated mission for monitoring climate gases. To support the analysis, the measurements are put in parallel to those of the IASI sounder, which are extensively studied at ULB.

IASI (Infrared Atmospheric Sounding Interferometer) is a nadir looking thermal infrared sounder onboard the meteorological platform MetOp, launched by Eumetsat in October 2006 and that will provide 15 years of global scale observation (Clerbaux et al, 2009). Its primary objective is to deliver continuously and on the long-term data to support not only operational meteorology but also environmental forecasting and global climate change monitoring.

With a global coverage and substantial sampling, this sounder uses the thermal infrared range to probe the composition of the atmosphere. By having a global coverage, it allows to follow the spatial and time evolution of the atmospheric trace gases as well as the aerosols. IASI benefits from a near real-time discrimination of the data (between the moment that the measurements are made by the satellite and the moment they are available to the user, on ground) which enhances scientific return and enables operational application. IASI consists in a Fourier Transform Spectrometer (FTS) associated with an imaging instrument to detect clouds and aerosols.

TANSO (Thermal And Near infrared Sensor for carbon Observation) on board GOSAT (Greenhouse gases Observing SATellite) is also a nadir looking sounder, launched in January 2009 by the Japanese Aerospace Exploration Agency and that is specifically designed to monitor CO_2 and CH_4 from space during its lifetime of 5 years (Kuze & Suto, 2008). This way, it intends to estimate the greenhouse gases source and sink in a sub-continent scale and verifying if the requirements of the Kyoto Protocol are being achieved. The Kyoto protocol aims to the reduction of the greenhouse gases in the atmosphere during the first period of commitment (2008-2012). As IASI, TANSO is a FTS with high optical throughput and spectral resolution, detecting shortwave infrared (SWIR) and thermal infrared (TIR) spectra. It is coupled to an imaging instrument to detect clouds and aerosols.

This work is thus intended to look deeper in the spectra recorded by TANSO in order to estimate the extent of available in comparison with IASI. In particular, we aim to analyze the possible gain of having higher spectral resolution to monitor trace gases with weak absorptions. Additionally, we intend to examine the measurement in the SWIR and determinate how they can be used for atmospheric chemistry analysis. The species we are more interested in are nitrogen compounds and especially ammonia (Clarisse et al, 2009), for which the first observations from space have recently been made. Specifically, we intend to use the satellites' measurements of NH_3 to try to inform on the nitrogen cycle, study the NH_3 seasonal variation above a specific location and what can lead to such variation, and also infer if it is possible to detect patterns of the diurnal cycle.

The importance of monitoring the nitrogen cascade is related with the important implications that it has in our planet. Even though nitrogen is an essential element for life on Earth, along with oxygen, it can be dangerous for living organisms. The inert form (N_2) is harmless but the reactive form can be deleterious when it accumulates and cycle in the air, soils or water.

During the last century, the mass production of reactive nitrogen has increased very much due to the needs of society nowadays, which is reflected in the need for food and energy that lead to several environmental issues (Galloway & Aber, 2003), such as:

- Eutrophication and acidification of soils and water
- Air quality
- Climate change

- Malnutrition

The capabilities of satellites to provide global-scale measurements of reactive nitrogen in the environment offers an important opportunity to better quantify nitrogen sources, follow transformation and transport. By using also chemistry models, this would help to better understand the impacts of these reactive species on human and ecosystems health on a regional or global scale.

This work is organized as follows. In the first Chapter we provide a detailed description of the TANSO-GOSAT mission, including mission objectives and technical specifications, and recall in comparison some of the relevant characteristics of IASI-MetOp. The second Chapter provides the theoretical elements of the atmospheric radiative transfer, which are needed to analyze the satellite measurements in both the thermal and short-wave infrared spectral regions. The specific objectives of this work are provided in Chapter 3; Chapter 4 provides the principal results and the discussion in particular with regard to reactive nitrogen monitoring with GOSAT, but also including a detailed analysis of radiometry accuracy (comparing of the TANSO radiances to the IASI ones) and spectral calibration. Chapter 5 brings conclusions and the perspectives for future work.

Chapter 1

TANSO/GOSAT and IASI/MetOp satellites sounders

1.1 GOSAT science objectives

The Greenhouse gases Observing SATellite (GOSAT, "IBUKI" as it was named by its Japanese creators) was launched on the 23rd of January, 2009 (Yokota, et al., 2009). This project was born from a co-operation between three different Japanese entities each one with their own responsibilities: the Ministry of the Environment (MOE), the National Institute for Environmental Studies (NIES), and the Japan Aerospace Exploration Agency (JAXA). The role sharing is illustrated in figure 1.

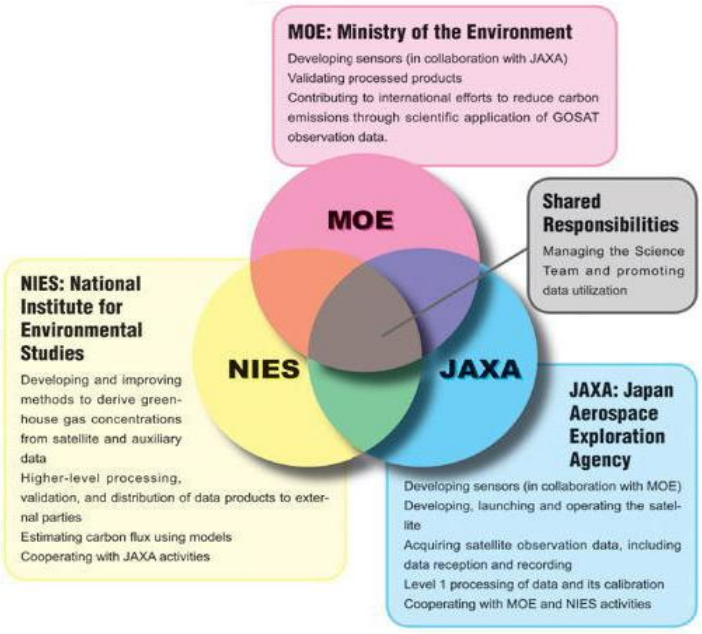

Fig. 1 – Role sharing in the GOSAT project. (http://www.gosat.nies.go.jp/)

GOSAT is the only satellite mission fully dedicated to measuring atmospheric greenhouse gases, and especially CO_2 and CH_4, for the benefit of climate science and policy. By the time that GOSAT was being developed, in 2003, there wasn't accurate information of how the greenhouse gases are geographically distributed on the earth and/or how they behave seasonally on the global scale. The decision of launching the first satellite in the world to monitor the greenhouse gases (carbon dioxide, CO_2, and methane, CH_4) was made with two specific purposes:

- The first scientific objective of GOSAT lies in the need to make accurate estimate of sources and sinks of carbon dioxide (CO_2) and methane (CH_4) on a sub-continental scale. With this, the aim is to contribute for a better understanding of climate issues by identifying the type and the geographical distribution of those fluxes (i.e., sources and sinks). Using this data, improved knowledge about the global distribution and seasonal variations of the greenhouse gases are expected. In turn, this should improve our understanding and modeling of the global carbon cycle and its influences on the climate.
- The second scientific objective of GOSAT concerns to the expansion of the existing earth observation satellite technology, developing new methods and technologies for greenhouse gases measurements, that should benefit future earth observing satellites.

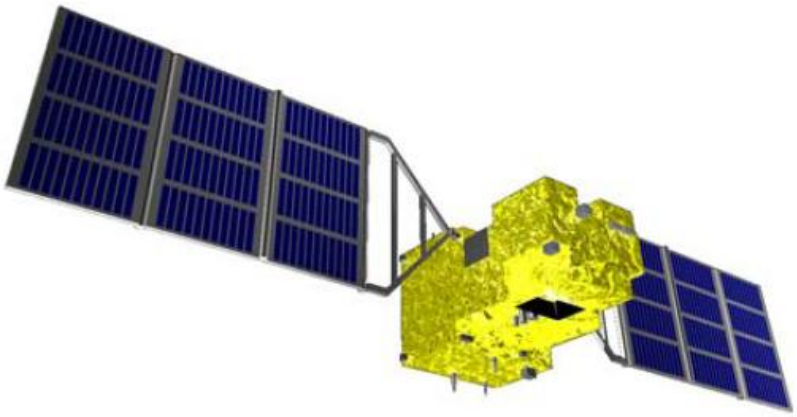

Fig. 2 – Overview of GOSAT in orbit. (http://www.gosat.nies.go.jp/)

1.2 GOSAT orbit and TANSO instrument

GOSAT is a sun-synchronous satellite that flies at an altitude of 666 km, approximately. A sun-synchronous satellite has a geocentric orbit that combines altitude and inclination in a way that the satellite ascends or descends over one given point of Earth's surface at the same local mean solar time.

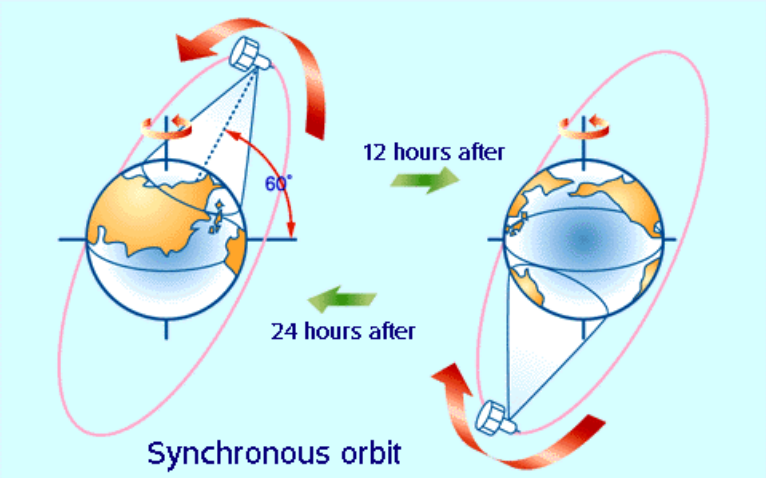

Fig. 3 – Illustration of a sun-synchronous orbit. Figure courtesy of the National Space Agency of Japan (NASDA)

GOSAT does 14+2/3 revolutions per day and so doing, after a three-day period (44 revolutions in total) it will be back at the same location. The onboard instruments have an external field of view of 15.8 mrad, corresponding to a footprint of 10.5 km approximately (diameter field of view for observation) at the surface, see figure 4.

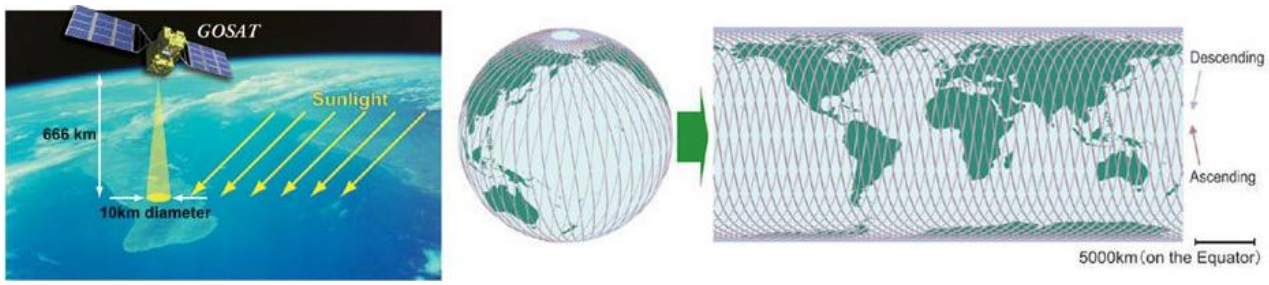

Fig. 4 – GOSAT observation and orbits. (http://www.gosat.nies.go.jp/)

Onboard GOSAT there are two instruments: The Thermal And Near infrared Sensor for carbon Observation-Fourier Transform Spectrometer (TANSO-FTS) and TANSO-Cloud and Aerosol Imager (TANSO-CAI). These two sensors are placed in the earth-facing plane of the satellite, operating by a three-axis system that controls its altitude, allowing that they keep looking toward the geocentric direction.

1.2.1. TANSO-FTS

TANSO-FTS is the central instrument for this work. It observes visible and ShortWave InfraRed (SWIR) radiation of the sun reflected by Earth's atmosphere and surface as well as the Thermal InfraRed (TIR) radiation from the ground and atmosphere, as shown in the figure 5.

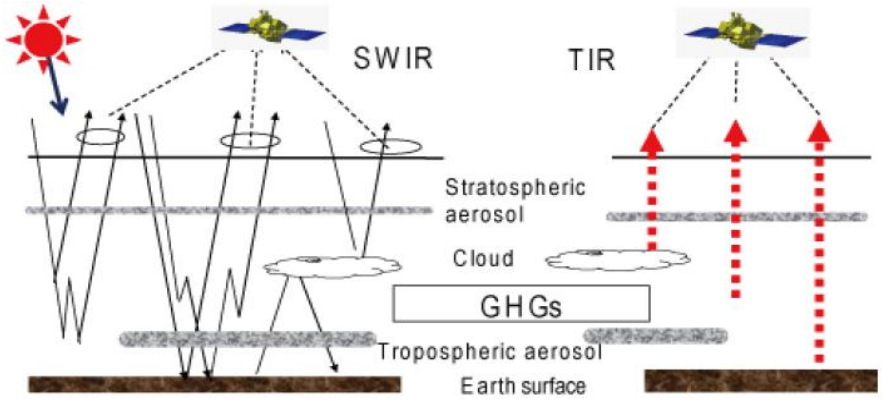

Fig. 5 – Radiance observation by TANSO in the short-wave and visible (left) using reflected/scattered solar radiation and in the thermal infrared (right). (http://www.gosat.nies.go.jp/)

While the satellite is moving, the FTS observes the same footprint during one interferogram measurement. In special observation mode, the instrument can make multiple observations for the same footprint, thereby improving the signal to noise ratio (SNR). TANSO-FTS does observations over the land on lattice points, which are made at a fixed angle interval in cross-track direction. The FTS detectors cover four bands, one corresponding to visible radiation, two corresponding to shortwave infrared, and one to thermal infrared radiation (see figure 7). Measurements are performed during day and night in the thermal infrared and only during day-time in the SWIR, as these observations require solar radiation. The wide spectral coverage allows detecting numerous molecular bands and infer accurate concentration retrievals.

Note that, there's a significant difference in the reflected character of sunlight over land and over big water surfaces, like oceans or lakes. Water reflects sunlight specularly in certain directions increasing the radiance signal and hence signal-to-noise. Water bodies are particularly interesting for the shortwave infrared during day-time.

Table 1 presents the characteristics of the TANSO-FTS.

Table 1 - Characteristics of the TANSO-FTS instrument.

	Band 1	Band 2	Band 3	Band 4
Band name	Visible	SWIR	SWIR	TIR
Spectral range	12900 – 13200 cm^{-1}	5800 – 6400 cm^{-1}	4800 – 5200cm^{-1}	700 – 1800cm^{-1}
	0.758 – 0.775µm	1.56 – 1.72µm	1.92 – 2.08µm	5.56 – 14.3µm
Spectral resolution	0.2cm^{-1}			
Target species	O_2	CO_2, CH_4	CO_2, H_2O	CO_2, CH_4
Field of view	15.8mrad (footprint: 10.5km)			

TANSO-FTS is an instrument based on the principle of a Michelson interferometer (figure 6); the incoming beam is divided in two beams at 90º that are each reflected by a mirror at the end of the path. In a typical Michelson interferometer, one of the mirrors is moving, so the optical paths are different for the beam. It is such that when they recombine after reflection, positive or negative interference is created. An interferogram is created by changing continuously these path lengths. The inverse Fourier transform of the interferogram, generates the light source spectrum (see hereafter). Through this method, the spectra can be acquired in a wide spectral range with at a high spectral resolution.

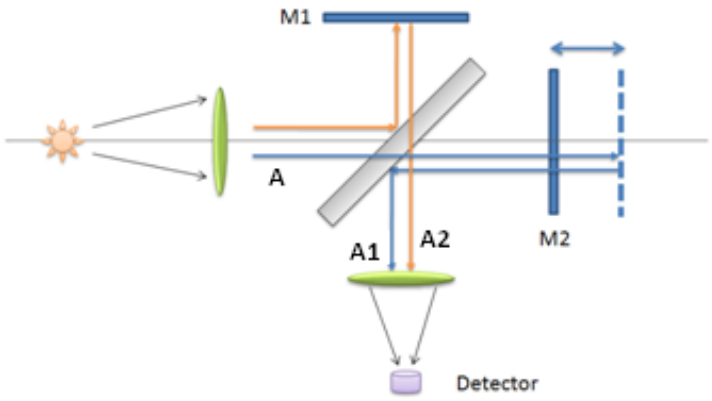

Fig. 6 – Diagram of a Michelson interferogram.

The figure 6 shows a diagram of a Michelson interferometer, where M1 is a fixed mirror and M2 is a moving mirror. In the specific case of TANSO-FTS, however, both mirrors are connected by a swinging arm so that they move the same distance but with opposite phases. This way, the scan speed is increased due to a doubled path difference. The interferometer achieves high spectral resolution and the increased speed allows high spatial resolution and sampling without sacrificing any of these characteristics.

The mathematics behind a classical Michelson such as described in figure 6, is as follows. If we consider a ray of light, A, coming from a source, one part will be reflected, A2, and go to

the mirror 1, M1, that will be detected and the other part will get through the separator, A1, and be reflected by the mirror 2 (M2). These can be written as:

$$A = A_0 \exp i\left[\omega t - \mathrm{k}\cdot\mathrm{r}\right] \tag{1.1}$$

$$A_1 = A_0 r_s t \exp i\left[\omega t - \mathrm{k}\cdot\mathrm{r}_1\right] \tag{1.2}$$

$$A_2 = A_0 r_s t \exp i\left[\omega t - \mathrm{k}\cdot\mathrm{r}_2\right] \tag{1.3}$$

Where A_0 the amplitude of the incident beam, r_s is the reflectance of the separator, t the transmittance, ω the pulse beam, r_1 and r_2 the distances between the separator and M1 and M2, respectively. This way, the intensity detected by the detector is given by

$$I(\delta) = \left|A_1(\delta) + A_2(\delta)\right|^2 \tag{1.4}$$

$$I(\delta) = B\left[1 + \cos(\mathrm{k}\delta)\right] \tag{1.5}$$

Where $B(\tilde{\upsilon}) = 2A_0^2\left|r_s\right|^2\left|t\right|^2$, $\delta = r_2 - r_1 = 2d$, $k = 2\pi\tilde{\upsilon}$ and $\tilde{\upsilon}$ the wave number. Thus, the interferogram is given by

$$I(\delta) = \int_0^\infty B(\tilde{\upsilon})\left[1 + \cos(2\pi\tilde{\upsilon}\delta)\right]d\tilde{\upsilon} \tag{1.6}$$

$$I(\delta) = \int_0^\infty B(\tilde{\upsilon})d\tilde{\upsilon} + \int_0^\infty B(\tilde{\upsilon})\cos(2\pi\tilde{\upsilon}\delta)d\tilde{\upsilon}$$

$$I(\delta) = I'' + I'(\delta) \tag{1.7}$$

The term dependent of the δ can be written as the Fourier transform of the spectral distribution. So, by applying the inverse Fourier transform the spectral distribution is obtained:

$$B(\tilde{\upsilon}) = 2\int_0^\infty I'(\delta)\cos(2\pi\tilde{\upsilon}\delta)d\delta \tag{1.8}$$

In fact a real interferogram is never obtained over an infinite path difference but to a limited maximum, L. The real spectrum is calculated after applying the inverse Fourier transform over the infinite path, convolved by an instrumental function that account for the truncation of the interferogram to a finite path length. The latter has the form of a sinus cardinal function (Hurtmans, 1995):

$$H(\tilde{\upsilon}) = 2\int_0^L I'(\delta)\cos(2\pi\tilde{\upsilon}\delta)d\delta = 2LB(\tilde{\upsilon}) \otimes \mathrm{sinc}(2\pi L\tilde{\upsilon}) \tag{1.9}$$

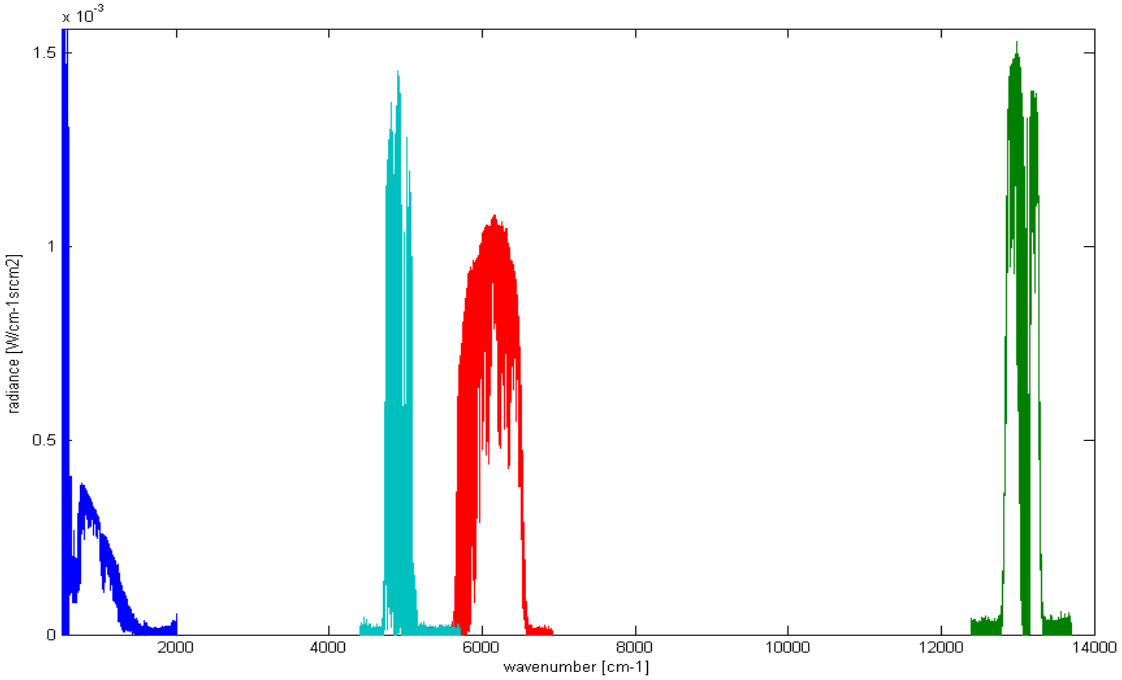

Fig. 7 - Example of a local day-time GOSAT spectrum in the four different spectral bands, from the TIR to the visible. Note: the TIR band was multiplied by a factor or 30 for clarity.

1.2.2. TANSO-CAI

TANSO-CAI is a multi-channel imager (Table 2) which is used as supporting instrument to the FTS. It aims at identifying and characterizing clouds or aerosols in the instrument field of view. Depending on these (cloud/aerosol coverage, optical thickness), the FTS data are either discarded if too much affected, or corrected. These corrections are of the utmost importance to provide measurements of CO_2 and CH_4 at the required accuracy.

Table 2 – Characteristics of the TANSO-CAI instrument. (GOSAT, 2009)

	Band 1	Band 2	Band 3	Band 4
Center wavelength (μm)	0.380±0.005	0.674±0.005	0.870±0.005	1.60±0.01
Wavelength width (μm)	<0.02	<0.02	<0.02	<0.02

1.3 "Atmospheric Composition and Chemistry-Climate interactions with GOSAT": Background – from IASI and objectives

The main reason behind the present work is to exploit the measurements of TANSO-FTS in the continuation of the efforts made at ULB to monitor atmospheric composition using infrared satellite sensors, and especially IASI. These objectives have been laid in the proposal "Atmospheric composition and Chemistry – Climate interactions with GOSAT" which was selected as PI contribution in the GOSAT mission project, giving us full unrestricted access to the measurements. Among the specific objectives of the proposal, the comparison of the TANSO-FTS measurements with those of IASI is an essential first step. The IASI instrument is shortly described hereafter.

1.4 IASI/MetOp instrument and mission

The Infrared Atmospheric Sounding Interferometer (IASI) is a nadir looking sounder onboard MetOp (METeorology OPerationnal) meteorological payload. It was launched in 2006. IASI consists in a FTS associated with an imaging instrument, to measure thermal infrared spectra.

IASI was developed in cooperation between CNES (Centre National d'Etudes Spatiales) and Eumetsat (European Organization for the Exploitation of Meteorological Satellites) in order to measure with unprecedented accuracy and sensivity a series of meteorological parameters, and in particular temperature and humidity. Apart of these objectives, IASI aims to measure several trace gases such as O_3, CH_4 and CO, to make an important contribution for the study of the global atmospheric pollution (Clerbaux et al, 2009).

Fig. 8 – MetOp and IASI (http://www.esa.int/)

As TANSO, IASI is a Fourier Transform Spectrometer (FTS) that is associated to an imaging instrument. It measures the emitted TIR spectrum by the system Earth-atmosphere. The carrying MetOp platform has a polar sun-synchronous orbit at an altitude of 817 km with an inclination of 98.7° to the equator. The measurements are taken twice a day, at 9h30 (21h30 in the evening) local time and each orbit takes 101min to be completed. After a whole day, IASI has thus made 14 orbits, similarly to GOSAT.

A major difference between IASI and TANSO lies in the spatial and temporal sampling, with IASI being designed to achieve global coverage at high resolution and sampling to benefit meteorological applications. In order to achieve a global coverage, IASI observes Earth with an angle of 48.3° on both sides of nadir to cover a 2500 km swath across the satellite track. There are a total of 30 fields of views in the swath and each is composed of a matrix of 2x2 pixels. The spatial resolution corresponds to the size of a single pixel, which has a 12km diameter on the ground at nadir. With the global coverage twice daily, IASI provides close to 1.3×10^6 observations per day (in comparison with, approximately, 1×10^4 with GOSAT).

The IASI instrument is equipped with several detectors in order to cover the spectral range that goes from 645 to 2760 cm^{-1}, and this way it is possible to include the strong absorption features from, among others, carbon dioxide (CO_2) around 15 μm, ozone (O_3) at 9.6 μm, strong water vapor ν_2 band and the methane (CH_4) ν_3 absorption band.

This broad spectral coverage without gaps is a unique feature of IASI. It is obtained by imaging the radiance onto three different detectors, separating the radiance signal in three bands; the first one between 645 and 1210 cm^{-1}, the second one from 1210 to 2000 cm^{-1} and the third one from 2000 to 2760 cm^{-1}. The IASI spectral resolution (FWHM) is between 0.35 cm^{-1} and 0.5 cm^{-1} for a FTS optical path of 2 cm, depending on the wavelength. For convenience, the standard radiance is apodized by a Gaussian function of 0.5 cm^{-1} FHWM and this can be considered as the apodized spectral resolution. In table 3 are specified the main features of IASI.

Is also worth to pointing out that the IASI instrument is calibrated in radiance from two common sources: a warm blackbody at 293 K and the cold space at 2.7 K. The IASI expected radiance accuracy is 0.5 K, which was recently confirmed on flight (Illigworth, Remedios, & Parker, 2009).

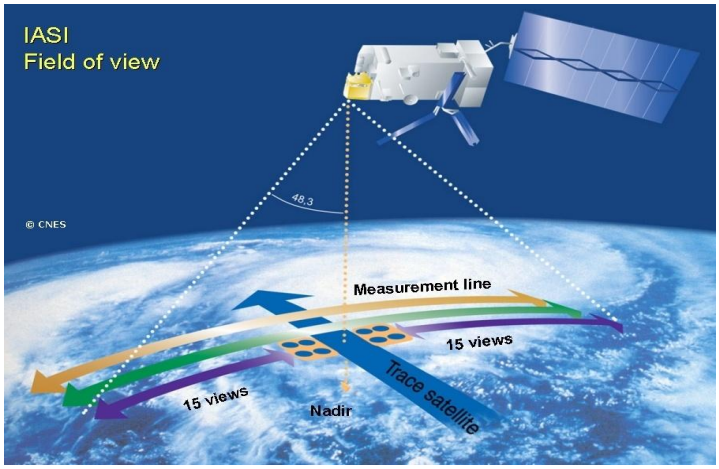

Fig. 9 – IASI observation mode. (http://smsc.cnes.fr/IASI/)

Table 3 – Characteristics of IASI. (Clerbaux et al, 2009)

Geometry of observation	Polar orbit (~ 800km); Nadir
Special coverage	Global and twice a day
Field of view	2x2 pixels corresponding to a footprint of 12km diameter.
Pixels/Scanning	120 (30 field of views)
Scanning	±48.3º
Spectral range	645 – 2760 cm^{-1}
Spectral sampling	0.25 cm^{-1} (8400 channels)
Spectral resolution	0.5 cm^{-1}
Lifetime	5 years
Data flow per day	1.300.000 spectra

IASI achieves measurements with a fairy low radiometric noise. It can be expressed in terms of either radiances or brightness temperature, which refers to the equivalent temperature of a blackbody radiator. This temperature can be obtained by inverting Planck function (see section 2.1). The noise in brightness temperature (ΔT – noise equivalent delta temperature) connects to the radiance noise $\Delta L_{\tilde{\upsilon}}(T)$ by,

$$\Delta L_{\tilde{\upsilon}}(T) = L_{\tilde{\upsilon}}(T)\left(\frac{hc\tilde{\upsilon}}{kT^2}\right)\left(\frac{1}{1-e^{-hc\tilde{\upsilon}/kT}}\right)\Delta T \qquad (1.10)$$

For a temperature of 280 K, the radiometric noise of IASI evolves from about $2\times10^{-6} W/m^2 \cdot sr \cdot m^{-1}$ for wave numbers between 650 and 1100 cm^{-1}, where the first spectral band takes place, to $1.5\times10^{-7} W/m^2 \cdot sr \cdot m^{-1}$ around 2100 cm^{-1} (figure 10), both values corresponding to noise equivalent delta temperatures of about 0.15-0.2 K of an equivalent blackbody at 280 K.

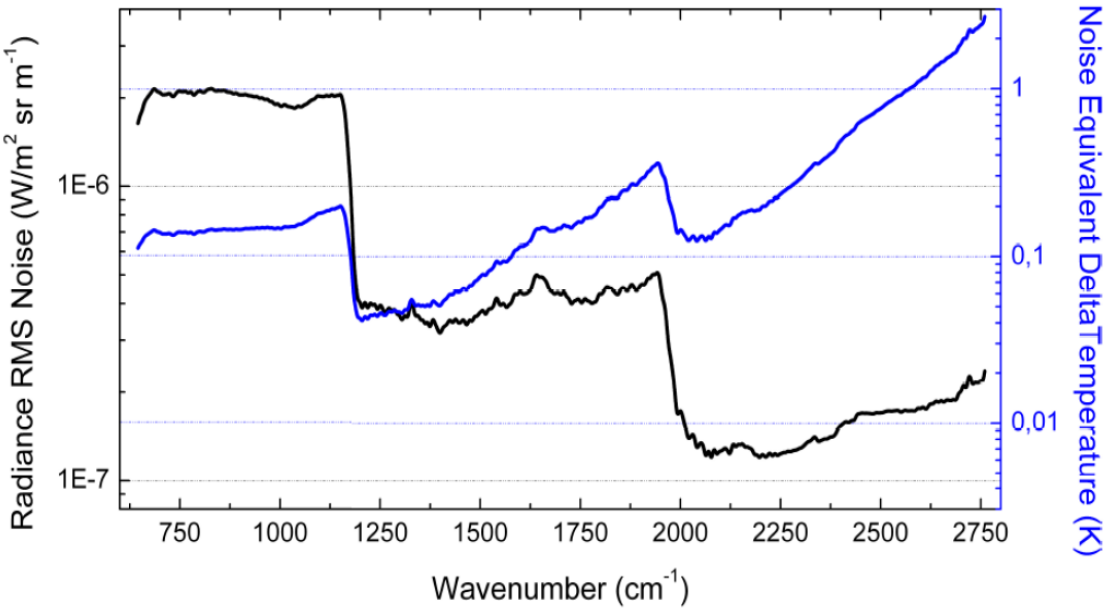

Fig. 10 – IASI radiometric noise over three spectral bands, in radiance units (black curve) and equivalent delta temperature (blue curve) (Clerbaux *et al*, 2009).

The figure 11 shows an example of an IASI spectrum where the radiance was normalized by dividing it by the Earth's blackbody function at the temperature of the observed area (top panel), along with contribution of molecular absorptions that can be divided in four different groups (three successive panels). In the two first groups are the strong absorbers with long lifetimes and important atmospheric concentrations. These include water vapor but also CO_2, N_2O, CH_4, O_3, CO and to lesser extent HNO_3. Then, in the third group there are the weak absorbers, some of which are detected only above emission sources or in concentrated plumes. These absorbers are CFC-11, CFC-12, SO_2, NH_3, HCOOH, CH_3OH, C_2H_4 and CH_3COONO_2 (PAN). It is worth pointing that aerosols can also be detected, for wave numbers between 700 and 1300 cm^{-1} (Clarisse, 2010).

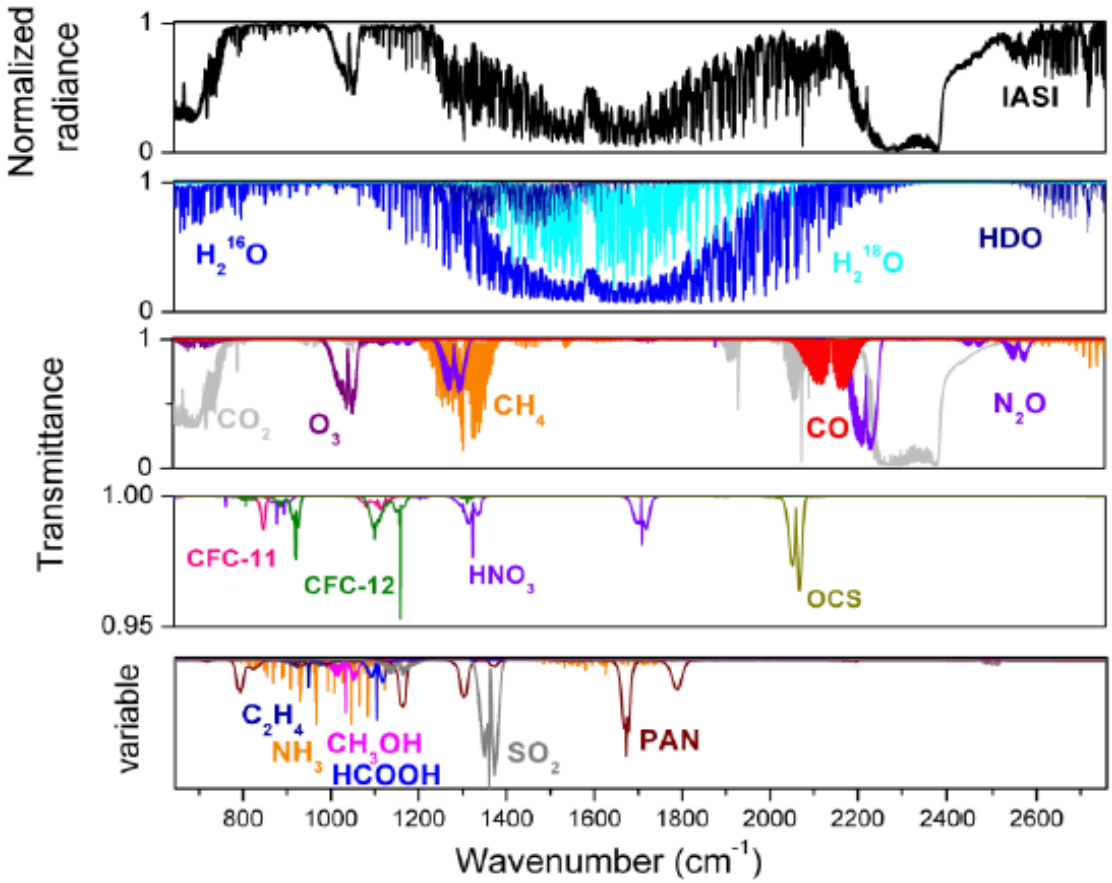

Fig. 11 – Example of an IASI spectrum in normalized radiance (top) and with individual molecular contributions highlighted (three following panels), in descending order of importance. (Clerbaux *et al*, 2009)

Chapter 2

Atmospheric radiative transfer (non-scattering atmosphere) applied to GOSAT

The remote sensing of the atmosphere is usually made by optical techniques and divided in two different groups: active and passive.

To better understand the work that was made and the analysis of the spectra obtained by TANSO and IASI satellites, this section discusses the physical principals inherent in the analysis of passive sounding in the infrared domain.

2.1 General formulation[1]

When an isothermal cavity is under thermodynamic equilibrium conditions, the radiation within this cavity is in equilibrium with the cavity walls and therefore, the spectral energy density depends only on frequency and temperature. If there's a small hole in the cavity, the emitted radiation will have the same form as radiation within the cavity and is called blackbody radiation.

Planck's function for a blackbody is given by the following equation:

$$B_\nu(T) = \frac{2h\nu^3}{c^2\left(e^{h\nu/k_BT} - 1\right)} \tag{2.1}$$

Where B_ν represents the spectral density in $W/m^2 \cdot Hz$, h is the Planck constant, ν the frequency, c the speed of light, k_B the Boltzmann constant and T the blackbody's temperature. At the temperatures of 288K and 6000K, Earth and sun that are the major source of radiation for the

[1] Reference (Andrews, 2000).

atmosphere, can be considered as blackbodies. The maximum of the radiation emitted by Earth belongs to the thermal infrared range while the radiation emitted by the sun covers the ultraviolet to the infrared, peaking in the visible (figure 12).

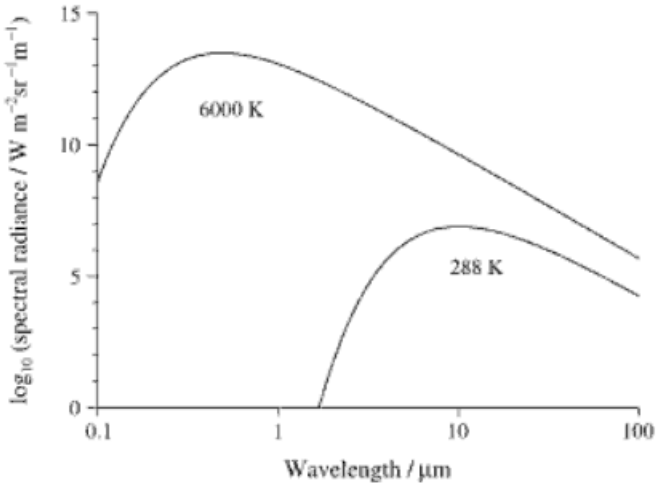

Fig. 12 – Illustration of blackbody curves at 288 K and 6000 K. Note the logarithmic scale of the black-body spectral radiance.

In nature a pure blackbody is rarely encountered but most real bodies can be fairly well described by a grey-body. The spectral emittance, e_ν, represents the fraction of spectral radiance emitted by a grey body in relation to a blackbody and therefore, $e_\nu \leq 1$. According with Kirchhoff's Law for a given temperature and frequency, $e_\nu=\alpha_\nu$ where α_ν represents the fraction of energy per unit of frequency interval falling on a body that is absorbed.

The quantity that describe the radiation collected by a remote sensing optical sounder is the spectral radiance, $L_\nu(\vec{r},\vec{s})$. It describes the flux of photons emerging from or arriving on a small area ΔA with unit normal $\vec{s}$, centered at a point $\vec{r}$ as shown in the figure 13 and it is measured in $W \cdot m^{-2} sr^{-1} Hz^{-1}$.

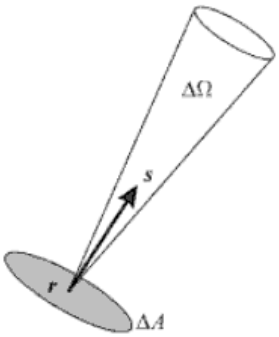

Fig. 13 – Illustration of the solid angle definition.

If the photons experience absorption or scattering in a small distance, ds, along the path – this happens for example in presence of an active gas along the radiation beam – then the spectral

radiance L_ν will decrease in ds. According with Lambert's law, the fractional decrease of the spectral radiance is proportional to the density of absorbing or scattering material encountered by the beam along the distance ds

$$dL_\nu = -\beta_e(s)\rho_a(s)L_\nu(s)ds. \tag{2.2}$$

With β_e being the extinction coefficient ($\beta_e = \beta_a + \beta_s$ where β_a is the absorption coefficient and β_s is the scattering coefficient) and ρ_a being the density of the active gas. But the gas itself can also emit photons at the frequency ν and in that case an additional term should be added to the previous equation. We have therefore obtained the Radiative-transfer equation:

$$\frac{dL_\nu}{ds} = -\beta_e\rho_a(L_\nu - J_\nu) \tag{2.3}$$

Which is general form of the radiative transfer equation. In equation (2.3) $J_\nu(s)$ is called the source function.

For the sake of simplicity we will consider here only a non-scattering atmosphere, meaning free of clouds and aerosols. In that case, the scattering coefficient is $\beta_s = 0$ and the extinction coefficient is $\beta_e = \beta_a$. This way, the attenuation of the radiation through a thin layer of the atmosphere can be written as

$$dI_{abs} = -\beta_a \cdot I \cdot ds \tag{2.4}$$

While the radiation emitted by that same layer is given by

$$dI_{em} = \beta_e \cdot B \cdot ds = \beta_a \cdot B \cdot ds \tag{2.5}$$

Where B is the Planck function for a blackbody at a given temperature (equation (2.1)). So, in a non-scattering atmosphere, the net change of intensity is:

$$dI = dI_{abs} + dI_{em} \tag{2.6}$$

$$dI = -\beta_a \cdot I \cdot ds + \beta_a \cdot B \cdot ds$$

$$\frac{dI}{ds} = \beta_a(B - I) \tag{2.7}$$

This equation is the Schwartzschild's equation and is generic for all descriptions of absorption/emission processes in the atmosphere. Analyzing this equation makes it easily to infer if there is emission or absorption of radiation through a particular line of sight. That is, when $B-I>0$ means that the radiation emitted by the thin layer is greater than the attenuation of the radiation in that same layer, and thus, there is emission of radiation through the layer. On the contrary, when $B-I<0$ the effect of attenuation is greater than the emission and therefore, there is a decrease of radiance through the layer.

Considering the optical depth, τ, defined as the negative logarithm of the fraction of radiation that is removed from a beam by scattered or absorbed on a path, as a vertical coordinate since it corresponds to the vertical path from Earth's surface to outer space, we can manipulate the Schwartzschild's equation to become,

$$\frac{dI}{d\tau} = I - B \tag{2.8}$$

With $\frac{dI}{d\tau} = \frac{dI}{ds}\cdot\frac{ds}{d\tau}$, $\frac{dI}{ds} = \beta_a(B-I)$ and $\frac{ds}{d\tau} = -\frac{1}{\beta_a}$. If we multiply each side of the equation (2.8) by $e^{-\tau}$, we have:

$$e^{-\tau}\frac{dI}{d\tau} = e^{-\tau}(I-B) \tag{2.9}$$

$$e^{-\tau}\frac{dI}{d\tau} - e^{-\tau}I = -Be^{-\tau}$$

$$\frac{dI\cdot e^{-\tau}}{d\tau} = -Be^{-\tau} \tag{2.10}$$

Integrating along the optical depth, we have:

$$\int_0^{\tau'}\frac{dI\cdot e^{-\tau}}{d\tau}d\tau' = \int_0^{\tau'} -Be^{-\tau}d\tau' \tag{2.11}$$

$$\left[I\cdot e^{-\tau}\right]_0^{\tau'} = -\int_0^{\tau'} Be^{-\tau}d\tau'$$

$$I(0) = I(\tau')e^{-\tau} + \int_0^{\tau'} Be^{-\tau}d\tau' \tag{2.12}$$

This equation is another fully generic form of the atmospheric radiative transfer in a non-scattering atmosphere. It tells us that the radiance has two different components. The first one

represents the attenuated contribution of any radiation source in the far side of the path. For the case of a satellite in orbit looking at the surface, the term I(τ') is the intensity of Earth's surface while the term $e^{-\tau}$ is the transmittance from the whole atmosphere along the considered path. The second term of this equation (the integral) represents the integration of the thermal emission in each point along the line of sight, attenuated by the transmittance between the sensor and τ'.

2.2 Simplification for the TIR[2]

For the thermal infrared range it is possible to make a simplification, in the formulation of the radiative transfer considering that only the thermal emission/absorption are occurring (no reflection from the sun on the surface).

Therefore, in the case of a nadir looking satellite, like TANSO or/and IASI, that receives thermal infrared radiation from the Earth/atmosphere, and assuming that thermodynamic equilibrium prevails (meaning that the source function can be expressed by Planck's function $J_v = B_v$), the solution of the radiative transfer equation can be written as:

$$L_v = \int_0^{\infty} B_v(T(z)) \frac{\partial \mathrm{T}_v(z,\infty)}{\partial z} dz + B_v(T_s)\mathrm{T}_v(0,\infty) \tag{2.13}$$

Where $T(z)$ is the atmosphere's temperature, T_s is the surface's temperature and $\mathrm{T}_v(0,\infty)$ is the spectral transmittance between the z and the satellite. If there is no extinction along the path (in a non-scattering atmosphere) then the satellite only sees surface emission:

$$L_v = B_v(T_s) \tag{2.14}$$

That is, the radiative transfer equation is given by Planck function for a temperature T_s that it is the surface temperature. This way, it is possible to infer what the surface temperature is by inverting Planck function. More generally, radiance measured by the satellite can be converted into an equivalent temperature called brightness temperature, which would vary with the extinction signatures in the atmosphere.

$$T_B(v) = \frac{hv}{k \ln\left(1 + \frac{2hv^3}{c^2 L_v}\right)} \tag{2.15}$$

[2] Reference (Andrews, 2000)

2.3 Formulation for the SWIR; reflectivity of surfaces

As seen before, GOSAT takes measurements not only in the thermal infrared range but also in the shortwave range. The incident radiation is no more dominated by the Earth thermal radiation which rapidly drops to vanishing values below 4 μm (see figure 12) but by reflected solar radiation onto surfaces.

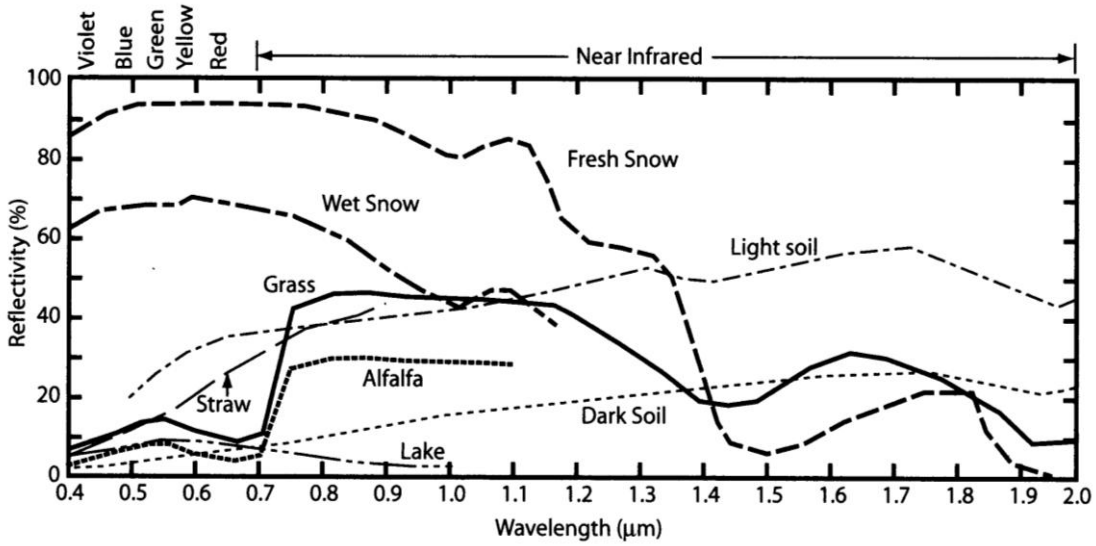

Fig. 14 – Example of surfaces' reflectivity. (Petty, 2006)

The figure 14, shows that the reflectivity of natural surfaces are strongly dependent of wavelength. Here we make the assumption that the reflectivity is independent of whether the sun shines, from East/West or North/South, which means that is azimuthally isotropic (referred to the horizon), and the dependence upon the zenith angle (referred to the vertical direction, 0°) can be ommited.

So, based on these assumptions it is possible to relate the monochromatic flux, which is the power per unit area per unit wavelength $\left(F_\lambda = \lim_{\Delta\lambda \to 0} \frac{F(\lambda, \lambda + \Delta\lambda)}{\Delta\lambda} \right)$, with the incident flux by the simple equation.

$$F_{\lambda,r} = r_\lambda F_{\lambda,0} \tag{2.16}$$

Where θ is the zenith angle, ϕ the azimutal angle and r_λ is the surface's reflectivity, which is only dependent of the wavelength. The reflectivity integrated over the shortwave is known as the albedo r_{SW}:

$$r_{SW} = 1 - a_{SW} \tag{2.17}$$

Where a_{SW} is the absorptivity in the shortwave range.

When the radiation that comes from the sun strikes natural surfaces, it can be reflected in several ways. What is usually done in modeling the radiative transfer is to simplify the formulation considering two different ways of reflection: specular or Lambertian.

In the case of a specular reflection, the flux incident is reflected with the same angle as it was incident on surface.

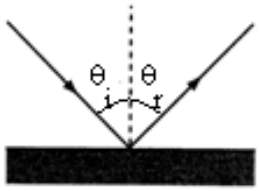

Fig. 15 - Specular reflection. (Petty, 2006)

For the second case of a Lambertian surface (schematized in the following figure), the reflection is equal in all directions.

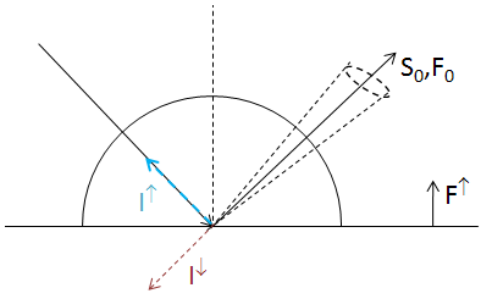

Fig. 16 - Lambertian reflection.

And then we have,

$$I^{\uparrow} = \frac{r_{\lambda} F_0}{\pi}, I^{\downarrow} = a_{\lambda} F_0$$

$$F^{\uparrow} = \int_0^{2\pi} \int_0^{\pi/2} I^{\uparrow}(\theta,\phi)\cos\theta \cdot sen\theta \cdot d\theta \, d\phi = \int_0^{2\pi} \int_0^{\pi/2} I^{\uparrow}(\theta,\phi)\cos\theta \cdot d\omega \quad (2.19)$$

Where dω is the solid angle. When the intensity is isentropic, that is when it is constant in all directions, we get to:

$$F^{\uparrow} = \pi \cdot I^{\uparrow} \quad (2.20)$$

When solving the radiative transfer equation in the SWIR the incident flux term $I(\tau')$ of the equation (2.12) that becomes the reflected flux (equation 2.16), which makes the formulation

somewhat more complicated. On the other hand, the second term of equation (2.12) disappears because the emission from atmospheric layers becomes insignificant.

Chapter 3

Objective of this research

This work is intended to provide a first analysis of the TANSO-FTS measurements in the thermal infrared and the short-wave infrared. The aim is to qualitatively evaluate the information that can be extracted regarding trace gases that are important for atmospheric chemistry, and that could complement measurements made by IASI thermal infrared sounder and others.

This objective is thus not in using GOSAT for its principal purpose (greenhouse gas monitoring) but more in trying to extract from it additional products of reference to the community of atmospheric researchers. The focus is given to reactive nitrogen compounds and in particular ammonia, for which there is a high interest in global remote sensing considering the lack of data.

Therefore and additionally, this works aims to evaluate the quality of TANSO-FTS measurements in the thermal infrared, where NH_3 signature is best seen.

Chapter 4

Results and discussions

In this Chapter are presented the results obtained in this work, as well as the inherent conclusions. First, are shown the results obtained for the short-wave infrared, followed by the thermal infrared results, radiometric cross-calibration between TANSO-FTS and IASI, spectral calibrations and instrument response function, and finally, the results regarding the monitoring of reactive nitrogen compounds.

4.1 TANSO measurements in the SWIR

4.1.1. Overview per band

In this section, the main goal is to identify the molecular signatures in a TANSO-FTS spectrum in the shortwave infrared range. For that, we used the radiative transfer program called Atmosphit that provides the user with an atmospheric ray tracing, a sophisticated formulation of atmospheric radiation and an optionally a fitting tool. Atmosphit solves the radiative transfer equation (2.12) line-by-line, using spectroscopic parameters from up-to-date databases and atmospheric profiles of pressure, temperature and gaseous concentration. The source function is modeled by a gray body in the thermal infrared. For modeling the short-wave infrared, an effective reflectivity is used for the reflected solar radiation.

Specifically, as inputs, Atmosphit needs four different files: the spectrum, a BMD file that contains the atmospheric base model (z (altitude), P (pressure), T (temperature) and VMR's (volume mixing ratios)) as well as the number of atmospheric levels and numbers of cross sections to be used, a FIN file that includes information on the geometry and the instrument specifications as well as the parameters to be fitted whenever relevant, and a High-resolution transmission molecular absorption database file (The HITRAN database) that compiles the spectroscopic parameters for 34 molecule. It is worth to take a look into the information contained in the FIN file, since this file contains most of the information that was manipulated to achieve the plots that will be shown ahead.

This file can be divided in three different parts: geometry (used to simulate the spectrum), spectrometer and molecular multiplicative model to fit. In the first group (geometry) is defined the limits of the atmosphere, the geometry type (ground or nadir) and some parameters about the light source (temperature and efficiency). For the second group (spectrometer) is present the information about the observed spectrum, that is: spectral limits and calibration factor parameters, the signal to noise ratio (SNR), the spectrum type (radiance or transmittance), the maximal optical path difference (MOPD) value of the interferometer, the apodization function and the field of view parameters and finally, the baseline parameters. Lastly, in the third group we find the information about the molecules and multiplicative factors to be simulated and fitted.

Table 4 summarizes the reference parameters used for the TANSO-FTS spectral simulations.

Table 4 – Parameters used to simulate the molecules' profiles.

	Apodization		**Internal FOV**	**Calibration**
Spectrometer	*ILS type*	*MOPD (cm)*	*Aperture*	4.58496×10^{-5}
	Boxcar	3.01 (FWHM = 0.2 cm^{-1})	0.4530°	
Baseline	*Spectrum type*	*Source temperature (K)*	*Blackbody efficiency*	*Ground reflectivity*
	Transmittance	320.67	0.9627	-
Geometry	*Limits of the atmosphere (km)*		*Line of sight*	*Earth Radius*
	0.0	666	Nadir + radiosity	6371.230

This way, for each spectral range – visible and shortwave infrared – the method used can be described in the following steps:

1. Change the concentration of each molecule, in the FIN file, that we want to simulate to produce detectable – but at the same time sometimes unrealistic – absorption signatures, as well as the other parameters that might be changed
2. Load the input files: spectrum, BMD file, FIN file and HITRAN file
3. Compute the spectrum line-by-line by solving the radiative transfer
4. Divide the blackbody function to the simulated spectrum to produce equivalent transmittances (normalized radiances)
5. Plot the obtained results for each molecule

After these five steps, we obtain the normalized transmittance for each molecule individually. We identify those species which contribute to the extinction of radiation and one (potentially for some) threshold by TANSO-FTS.

Figure 17, shows for the visible range, the molecules that are contributing to the TANSO-FTS spectrum used for this simulation. This spectrum was recorded above Pacific Ocean and thus representative of a background (unpolluted) atmosphere. In the visible, besides absorption

signatures of H_2O and week absorption of CO_2, there is also seen a strong signature of O_2 which is the molecule that TANSO-FTS aims to measure in this spectral band (see table 1).

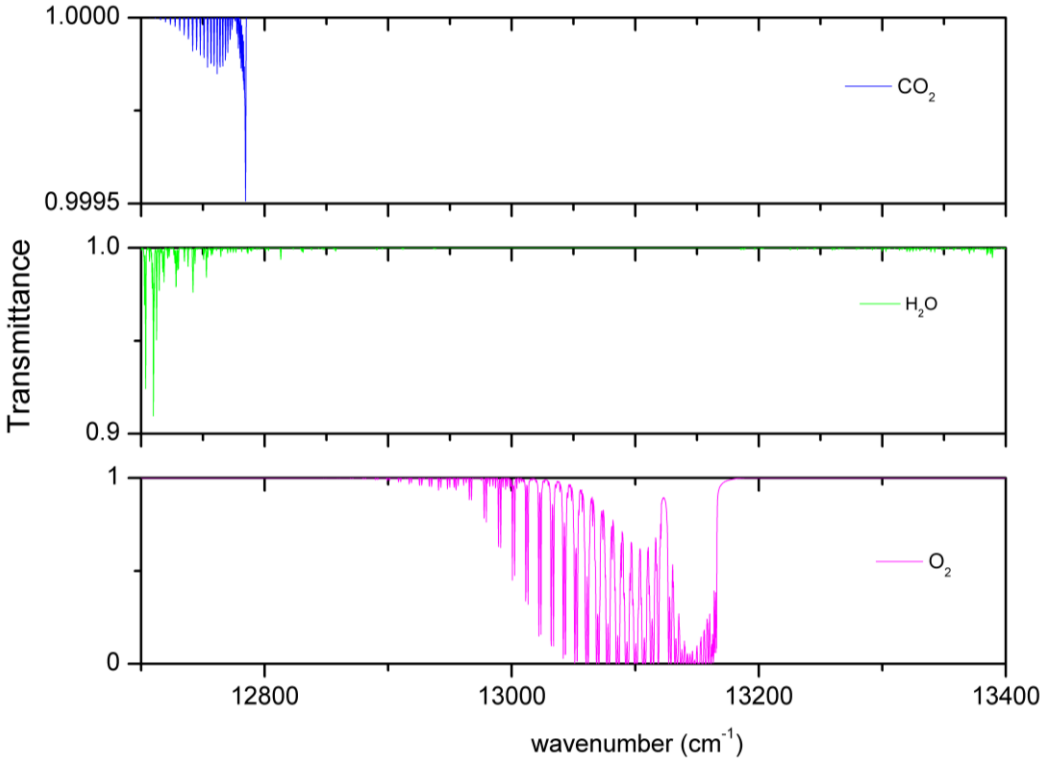

Fig. 17 – Individual molecular contributions highlighted for visible band; above Pacific Ocean.

For the second band, identified as SWIR 2, the target species are carbon dioxide and methane (see table 1). Those species strongly contribute to the TANSO-FTS spectrum. We could identify three more absorbing species in this spectral range: water, hydrochloric acid (HCl) and acetylene (C_2H_2), as shown in figure 18. For C_2H_2 and HCl the signatures only appear by largely increasing the species concentrations in our simulation. This means that they would only be detectable in particular conditions, above large emission sources (e.g. fires, volcanoes) (Clerbaux *et al*, 2009). More work is needed to check if these species would indeed be measurable by GOSAT.

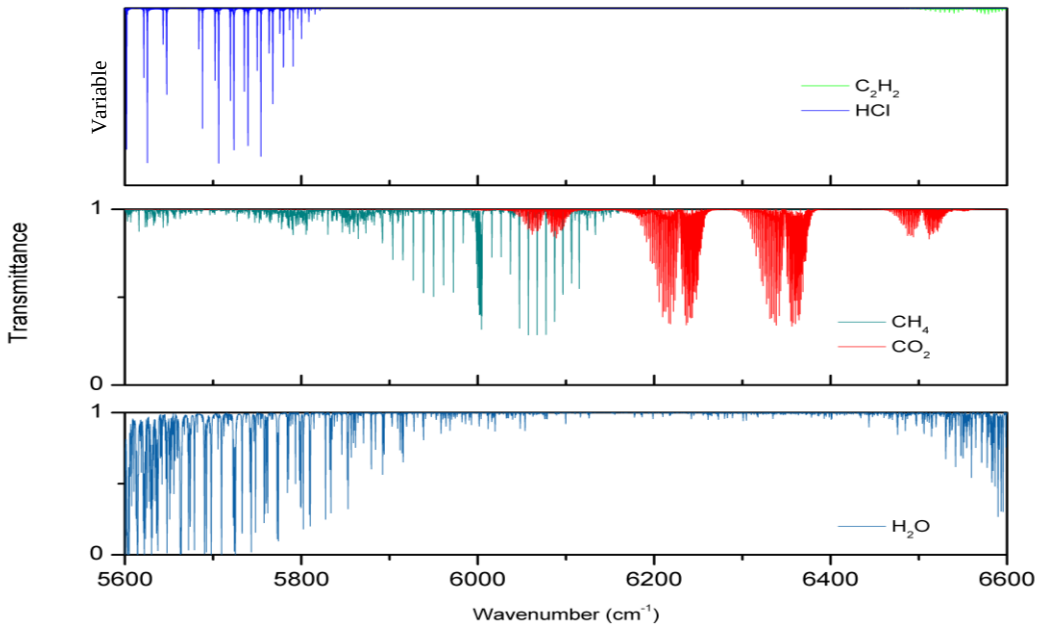

Fig. 18 – Individual molecular contributions highlighted for SWIR 2 band; above Pacific Ocean.

Interestingly, there is a feature in the SWIR spectrum that wasn't identifiable to the species listed in HITRAN, as shown in figure 19 centered around 6285 cm^{-1}. We are still looking for more information that can lead us to identify this molecular absorption shows up in every TANSO-FTS spectrum.

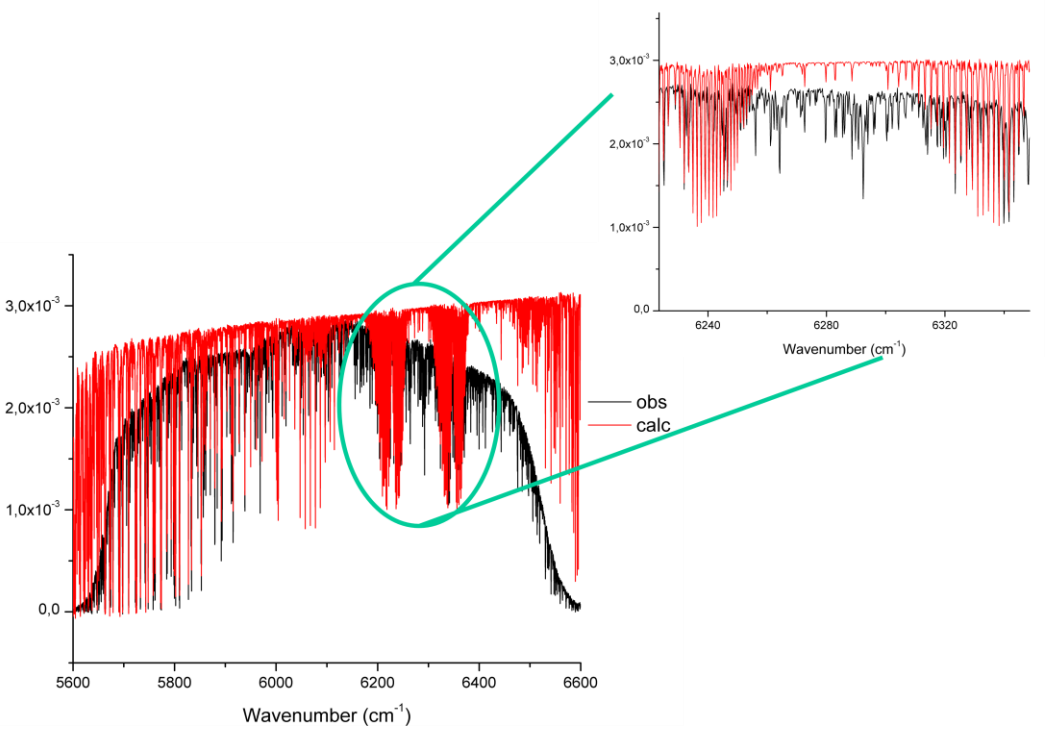

Fig. 19 - Unknown signature present in every TANSO-FTS spectrum.

For the second band of the shortwave infrared range, SWIR 3, the GOSAT target species are water vapor and carbon dioxide, which have indeed strong absorption (figure 20). In addition, that spectral band also includes contribution from CH_4, N_2O and to lesser extent O_3. Finally, although weak, there is a possible contribution of NH_3 to that part of the spectrum.

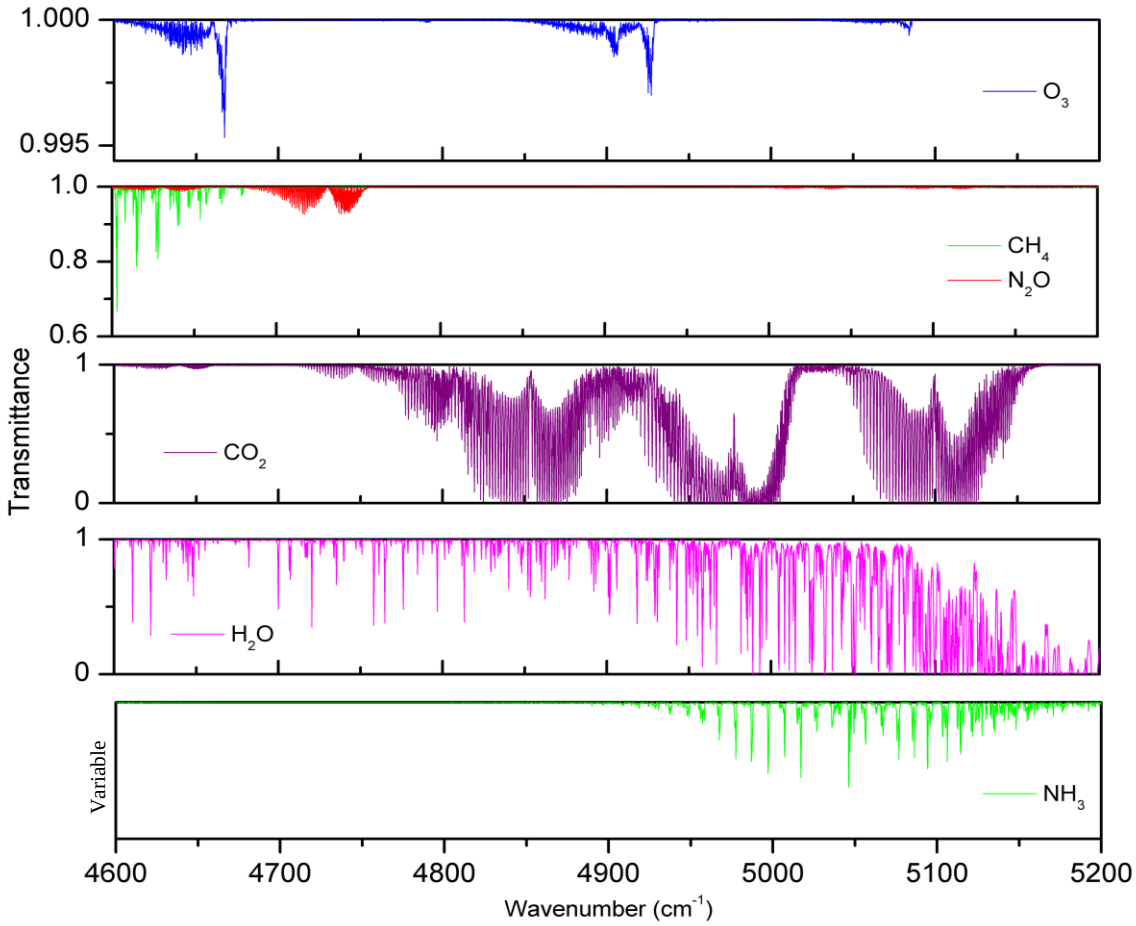

Fig. 20 – Individual molecular contributions highlighted for SWIR 3 band; above Pacific Ocean.

4.2 TANSO measurements in the TIR

4.2.1. Overview

Similarly to what is done above, here we present results from a set of forward simulations in the thermal infrared, to better characterize GOSAT measurements and provide a first basis of comparison to IASI. The spectra that is used for this purpose is the same as above, and was recorded above Pacific Ocean during the month of March 2010.

Like it was done for the shortwave infrared and visible bands, we used Atmosphit line-by-line radiative transfer model to compute the spectra, following the same methodology, to

highlight the principal absorption signatures in the spectra. All the parameters that were used are present in table 4.

The next figure shows the molecules that contribute to the spectrum in the thermal infrared range. It is similar to figure 11 (shown for IASI) but is specific to the TANSO-FTS instrument.

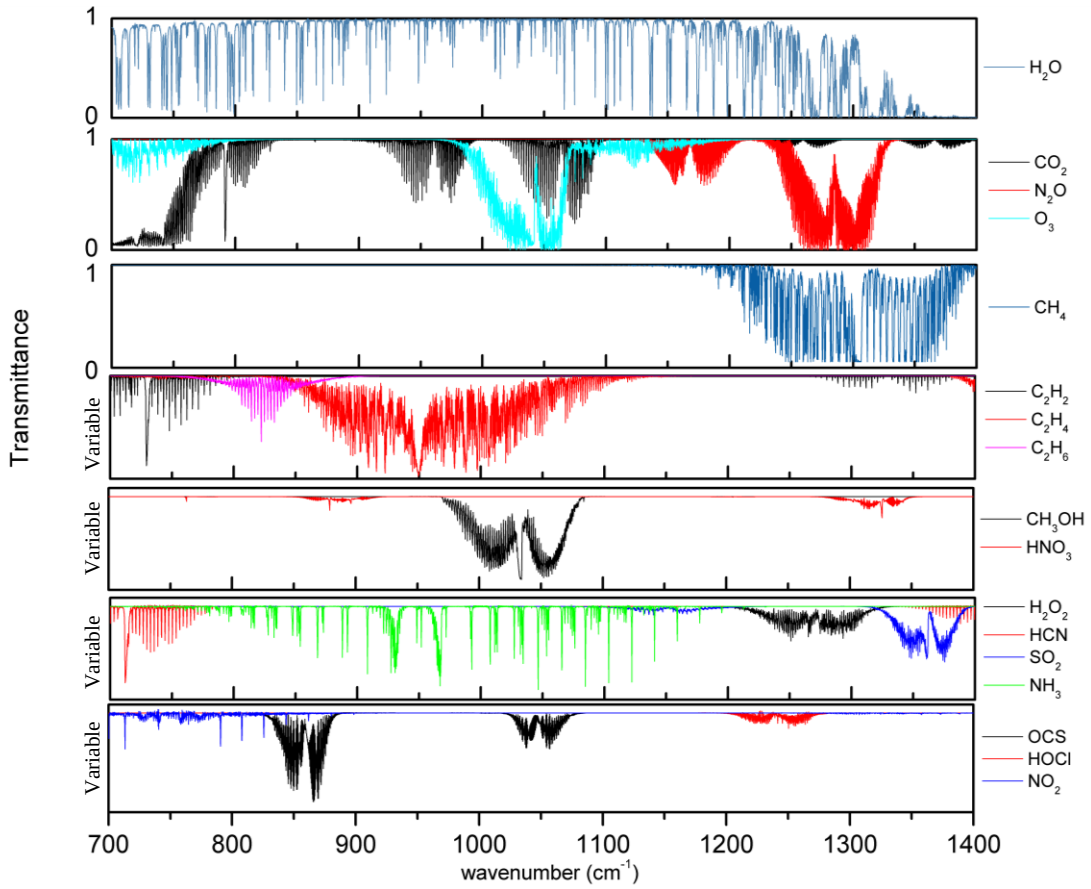

Fig. 21 – Individual molecular contributions highlighted for TIR band; above Pacific Ocean.

Within this range of wave numbers, the target molecules for GOSAT are the strong absorbers carbon dioxide (CO_2) and methane (CH_4). But as we know from IASI experience, there are a number of species that can be detected in high pollution areas or specific fire or volcanic plumes. (Clerbaux, 2009; Clarisse, Clerbaux, Dentener, Hurtmans, & Coheur, 2009). The identifiable species are grouped according to their absorbing strength in table 5.

Table 5 - List of some molecules absorbing in the TIR band of TANSO-FTS.

	CO_2	CH_4	O_3	N_2O	HNO_3	SO_2	NH_3	CH_3OH	C_2H_2 C_2H_4 C_2H_6	OCS
Strong absorber	●	●	●	●						
Medium absorber					●					
Weak absorber						●	●	●	●	●

Besides the molecules that are listed in table 5, we also demonstrate the possible contribution of hydrogen cyanide (HCN), hypochlorus acid (HOCl), hydrogen peroxide (H_2O_2) and nitrogen dioxide (NO_2) even though all these molecules have very small features in the spectrum with variable transmittances. They are unlikely to be observed because of very strong interferences with the main absorbers (H_2O, CO_2, CH_4).

4.2.2. Radiometric cross-calibration between TANSO-FTS and IASI

The absolute radiometric accuracy of sounders as IASI or GOSAT is of the utmost importance because the atmospheric radiative transfer in the thermal infrared comes in propagating the Earth's source function through the atmosphere. A bias in the radiometric calibration induces errors on the entire radiative transfer, which translates in important errors on the retrieval of trace gas abundances. IASI was shown by cross-calibration with the AATSR instrument to meet its target absolute accuracy of 0.5 K (Illigworth, Remedios, & Parker, 2009). Here we provide a comparison between IASI and TANSO-FTS radiances, which is essential for future use of the TANSO infrared radiances for chemistry applications.

For a more accurate comparison in terms of radiance, it's better to consider surfaces with constant emissivity, good temporal and spatial agreement, observed with similar fields of view because radiances from thermal infrared range of the TOA vary strongly with the wavelength, temperature and emissivity of the surface, atmospheric temperature, atmospheric composition (especially humidity) and with clouds. Due to these reasons, the ideal surfaces are the oceans because their surfaces have a constant emissivity and small temporal variations in temperature. This way, it's not advisable to use land surfaces since the temperature vary very rapidly and the radiance has a strong dependence of the angle of vision.

In order to do a cross-calibration, the brightness temperature measurements should indeed be done for a same geographical location (latitude and longitude wise) and for a similar time.

The method used in this work for the cross-calibration between IASI and TANSO-FTS has six steps, which are based on the considerations made before:

1. Selection of reference area above the Pacific Ocean: $-20^{o} < lat < -5^{o}$ and $-135^{o} < lon < -115^{o}$
2. Selection of 10 "clear windows" in each TANSO-FTS and IASI spectrum. We consider a clear window a spectral range where there's no absorption of any molecule for those wave numbers. They are reported on table 6.
3. Filter in latitude and longitude: only the spectra which have a difference in latitude and longitude less than 0.2º are analyzed
4. Time filter: only the IASI and TANSO-FTS spectra with a time difference less than 3 hours were analyzed
5. Calculate the Brightness Temperature (BT) for these spectra and compute the difference $BT^{IASI} - BT^{TANSO\text{-}FTS}$.
6. Filter in cloud coverage: only the IASI spectra with cloud coverage less than 15% were analyzed. IASI cloud information is provided operationally through the Eumetsat dissemination system. Cloud information from GOSAT were not available and hence, all TANSO-FTS data have been kept in the first phase of the analysis.

Table 6 – Clear windows used for the cross-calibration.

Wave number (cm^{-1})	**IASI channels**	**GOSAT channels**
786.25 – 790.75	566 – 580	712 – 734
822 – 823.5	709 – 715	892 – 899
829.5 – 834.5	739 – 759	929 – 954
866.5 – 869.75	887 – 900	1115 – 1131
898.5 – 904.25	1015 – 1038	1276 – 1305
1102 – 1105.3	1829 – 1842	2300 – 2316
1123 – 1133	1913 – 1953	2405 – 2456
1139 – 1147.5	1977 – 2011	2486 – 2528
1154 – 1163	2037 – 2073	2561 – 2606
1167 – 1172	2089 – 2109	2627 – 2652

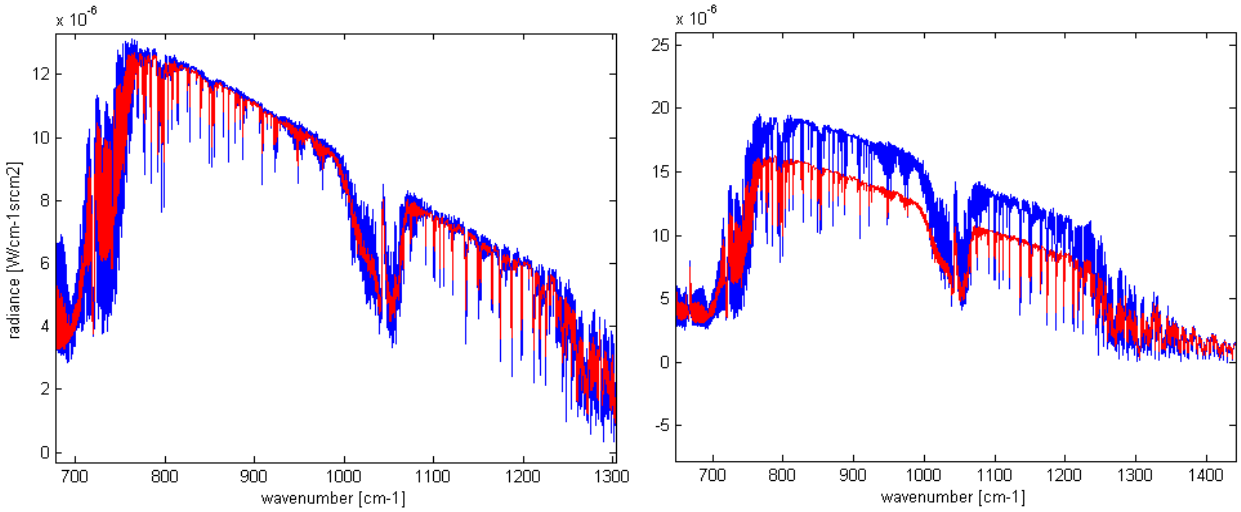

Fig. 22 – Night-time spectrum for the thermal infrared range above sea. Left panel: good agreement between TANSO-FTS (blue line) and IASI (red line). Right panel: bad agreement between both satellites.

Figure 22 shows a GOSAT and IASI spectrum collocated in space and time (see section 4.2.2) for the thermal infrared range, recorded during night-time. In the left panel, the spectra coincide well. A noticeable difference lies in the strength of the absorption lines, which is a direct consequence of the different spectral resolution. The higher resolution TANSO-FTS spectrum shows lines with larger strength. In the right panel, the spectra do not coincide that well in terms of their radiance values, likely pointing to remaining clouds in the dataset.

After applying the method described above, some statistics have been collected. First, we made a histogram with IASI and GOSAT day-time spectra that followed every step of the cross-calibration method, in order to see if there is any bias between the two satellite's data. According with the first histogram (figure 23 - left), we see that the majority of the TANSO-FTS spectra have brightness temperature between 2 and 3K above the IASI. With the same purpose, we compared IASI night-time spectra with GOSAT night-time spectra and as seen in the second histogram (figure 23 – right). On the contrary to day-time spectra, we do not see such a significant bias, with the distribution peaking just below 0 (the mean is at -0.7 K).

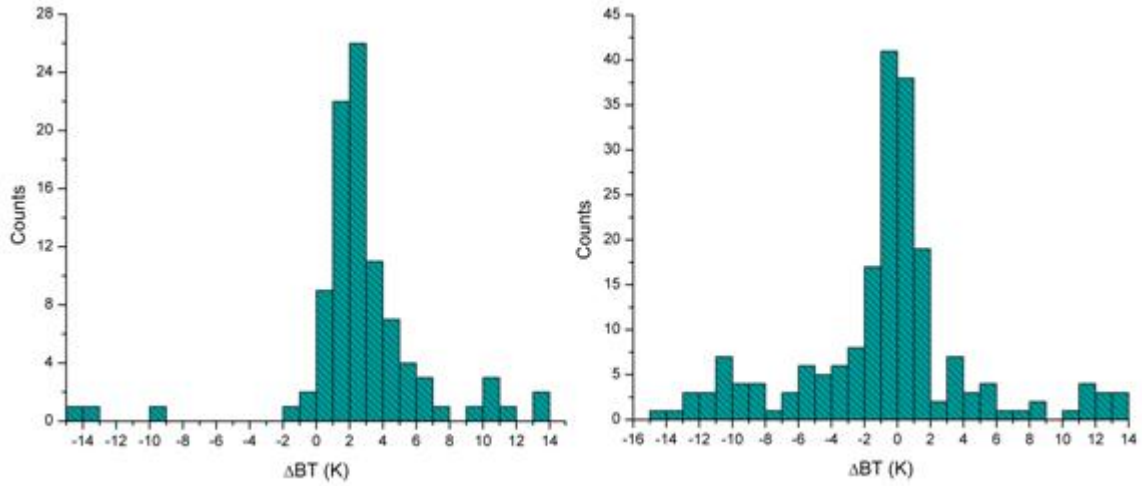

Fig. 23 – Left: histogram of brightness temperature differences for IASI and TANSO-FTS spectra occurred during day-time data. Right: same for night-time data (note: no time filter was applied).

Table 7 summarizes the results for the statistics made for both histograms data. Obviously the large standard deviation in both cases points to the presence of clouds or aerosol-containing scenes in on or another dataset, which leads to ΔBT values up to 15K.

Table 7 - Statistical values obtained for both set of data.

	IASI & GOSAT day-time	IASI & GOSAT night-time
Mean (K)	2.07716	-0.7009
Standard deviation (K)	7.2762	5.23924
Median (K)	2.2689	-0.1637

Based on the information from the histograms and statistics, we can say that there is a significant bias of GOSAT day-time spectra when compared with IASI spectra, for the same conditions (location, cloud coverage and time). The 2K bias can have large impact on the retrieval of trace gases and will have to be addressed urgently if the TANSO-FTS data are to be used for chemistry applications.

It is worth pointing that the histograms in figure 23 still contain a number of measurements for which the brightness temperature is lower than 290 K. This is of course not representative of the surface and likely points to the presence of low clouds or aerosols in the scene, despite the filtering of IASI data. In figure 24, the brightness temperature of IASI and TANSO-FTS are compared only for those scenes where the source is at 290 K or higher.

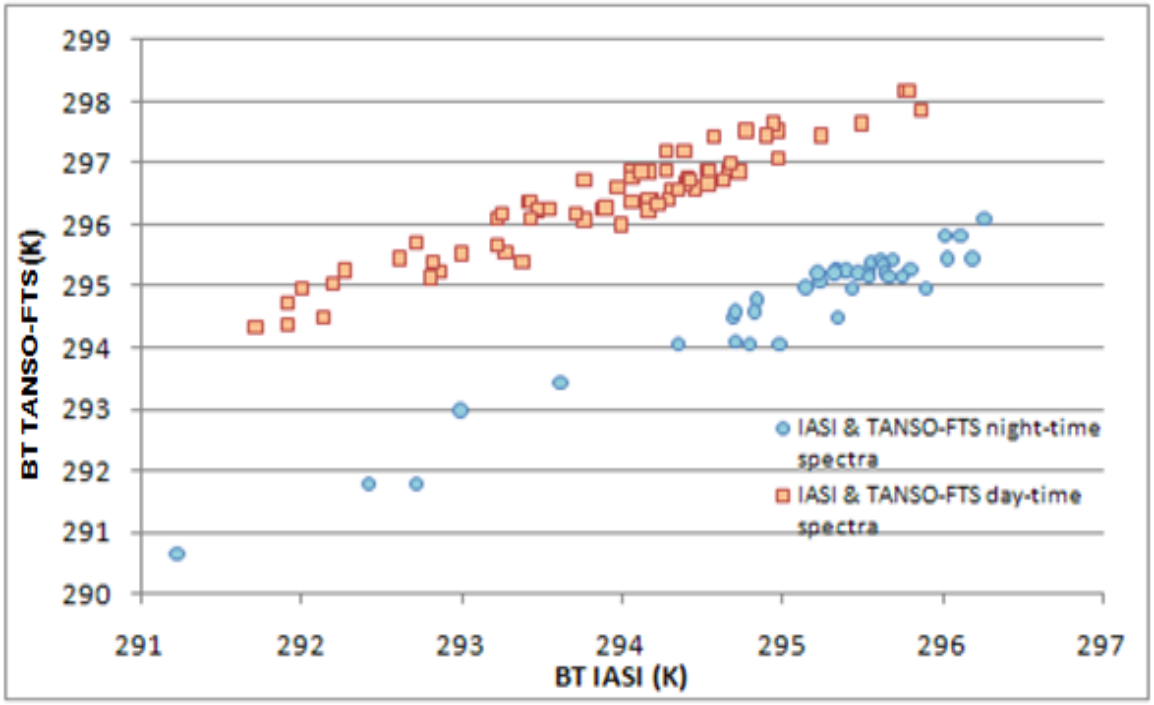

Fig. 24 - Relation between the brightness temperatures measured by both satellites.

As shown in figure 24, there is a linear relation between the values measured by both satellites, but with a remaining (~ 2 K) bias (TANSO-FTS > IASI) for the day-time data. On the contrary TANSO seems indeed to be biased low (~ 0.7 K) as compared to IASI for night-time.

4.2.3. Spectral calibrations and Instrument response function

In the same way that radiometric calibration is important, the spectral calibration and knowledge of the instrument response function is crucial in retrieving trace gases abundances from high-resolution measurements.

The instrument line shape function (ILS) depends on the theoretical spectral resolution (in a case of a FTS it depends on the optical path difference) and on the optical alignment of the interferometer. In the case there is no post apodization applied, the instrumental line shape of a FTS is a sinc function (Kuze & Suto, 2008).

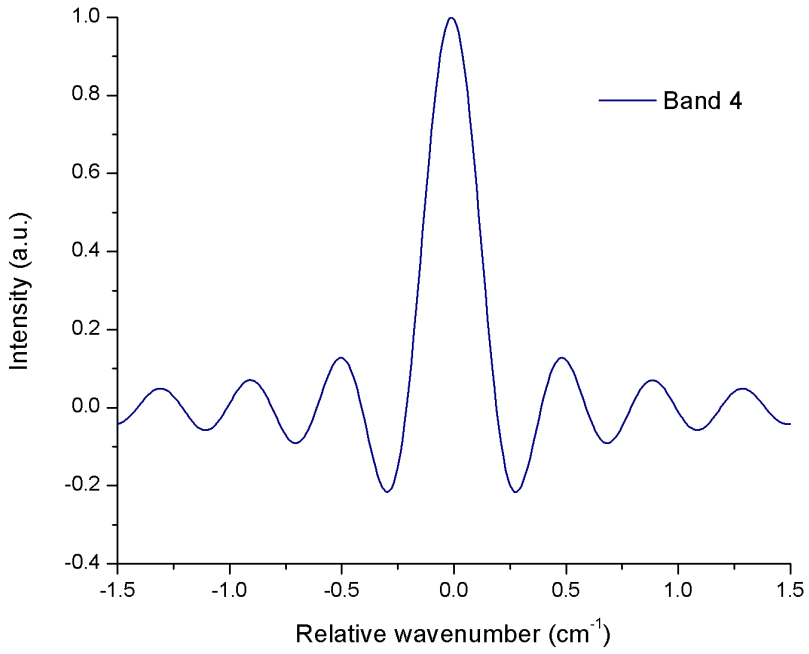

Fig. 25 – Instrumental line shapes for the TANSO-FTS TIR band, provided there is no misalignment in the spectrometer.

Using the program Atmosphit we have verified if the theoretical ILS function provides a good fit of the spectral lines. For that, is used a spectrum recorded above India on the 13th of April 2010 and the fit was performed for the spectral range between 900 and 915 cm^{-1}, with the parameters listed in table 8.

Table 8 - Parameters used to fit the spectrum.

	Apodization		Internal FOV	Calibration
Spectrometer	*ILS type*	*MOPD (cm)*	*Aperture*	4.58496×10^{-5}
	Boxcar	3.01 (FWHM = 0.2 cm^{-1})	0.4530°	
Baseline	*Spectrum type*	*Source temperature (K)*	*Blackbody efficiency*	*Ground reflectivity*
	Transmittance	320.67	0.9627	2×10^{-2}
Geometry	*Limits of the atmosphere (km)*		*Line of sight*	*Earth radius*
	0.0	666	Nadir + radiosity	6371.230

As can be seen from figure 26, although the sinc function reproduces fairly well the lines, there remain residual features larger than the noise around the strongest absorptions. This suggests some distortion of the instrumental line shape. Currently, we have no information on the TANSO-FTS line-shape besides the theoretical sinc function. As for the radiometric calibration this would need to be addressed before more geophysical studies are carried out.

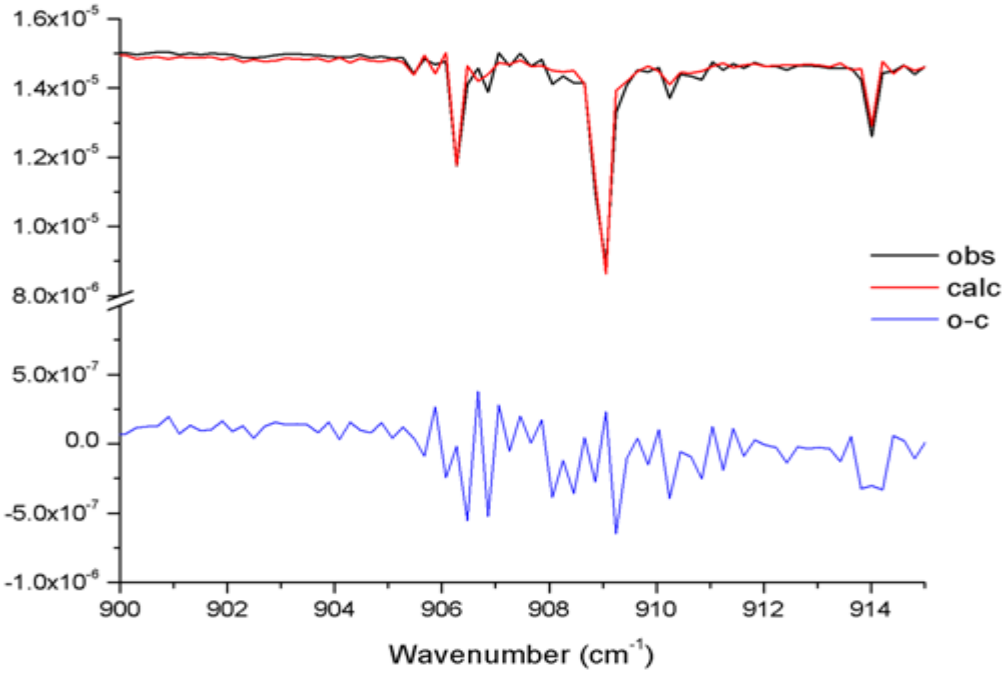

Fig. 26 – Spectral fitting of TANSO-FTS in a narrow portion of the TIR band.

4.3 On the potential use of TANSO/GOSAT for monitoring the nitrogen cycle

4.3.1. The perturbed cycle of reactive nitrogen[3]

In this section will briefly introduce the importance of reactive nitrogen cycle for the atmosphere and how complex it can be, as well as some ways to improve its impacts.

It is known that the total amount of nitrogen (N) in the atmosphere, soils and water is approximately 4×10^{21}g (4×10^{15} tons!), but most of it (99%) is not available for the majority (99%) of the organisms. The reason for this is that the nitrogen is present in the form of N_2 and this form cannot be assimilated by living organisms.

The nitrogen compounds can be divided in two groups: the non reactive, where N_2 is the only form of it, and the reactive forms, including all the biologically, photochemically and radiatively active N compounds in Earth's atmosphere and biosphere, that is accumulating in the environment, in all spatial scales, drastically since 1960 due to the largest increase in human production, compared with other systems. This accumulation can be due to different reasons:

1. Generalization of the cultivation of vegetables, rice and others, allowing the conversion of the non reactive form of nitrogen (N_2) into organic nitrogen through biological nitrogen fixation (BNF)
2. Burning of fossil fuels that converts N_2 and fossil N into nitrogen oxide (NO_x)
3. The Haber-Bosch process that is used to sustain food production and industrial activities. In this process the N_2 is converted into a reactive form of ammonia (NH_3): N_2 (g) + 3 H_2 (g) $\rightleftharpoons$ 2 NH_3 (g), with the latter used in ammonia-based fertilizers.

It is expected that the production of Nr keep increasing due to the increased population and the accumulation of Nr can contribute to:

- Serious respiratory illness, cancer and heart diseases induced by the production of tropospheric ozone (O_3) and aerosols
- Biodiversity reduction in some natural habitats
- Acidification that can also lead to biodiversity reduction in lakes in regions of the globe.
- Eutrophication (increased of chemical nutrients concentration in an ecosystem so that increases the primary productivity of the ecosystem), hypoxia (dissolved oxygen becomes reduced in concentration to a point detrimental to aquatic organisms living in the system) and loss of biodiversity and degradation in costal ecosystems.
- Global climate change and stratospheric ozone depletion, having serious impacts on human and ecosystems health.

[3] Reference (Galloway & Aber, 2003)

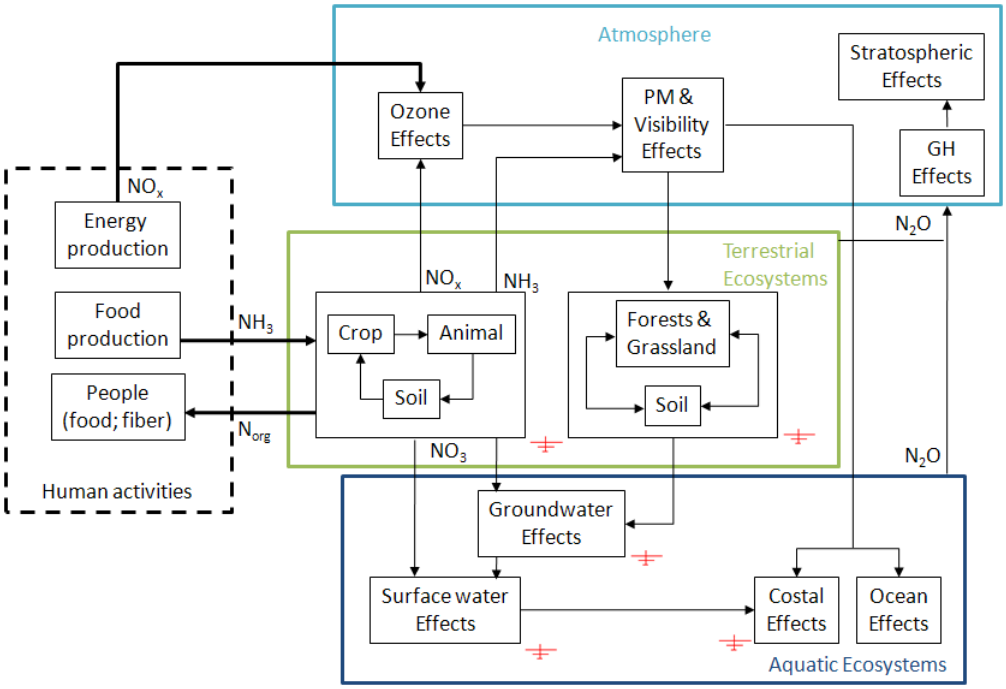

Fig. 27 – Nitrogen Cascade. (Galloway & Aber, 2003)

The cycle of reactive nitrogen is based on the multiple connections among the atmosphere and terrestrial and aquatic ecosystems. There are a multitude of impacts in each of these systems but because of the rapid cycling, once it starts, the source of Nr is now irrelevant and the consequences can be up to global. This is the nitrogen cascade introduced by (Galloway & Aber, 2003).

The atmosphere receives Nr coming from air emissions of NO_x and NH_3, N_2O – that has a residence time in the atmosphere of 100 years and it has been increasing at a rate of 0.25%/year – from land/aquatic ecosystems and of NO_x from burning fossil fuels. Short lived species such as NO_x and NH_x (NH_3 and NH_4^+) can accumulate in the troposphere on a regional scale, which some local effects were described above, but with global impacts that are also important to mention. One of these is the importance that NH_3 has by rapidly forming aerosols on the radiation balance and global climate, with likely a dominating cooling effect.

4.3.2. Measuring NH_3 from GOSAT: method

GOSAT is a satellite that was built especially to measure carbon dioxide and methane but as we found out, it provides measurements that can be used to inform on other atmospheric species, including some of the important reactive nitrogen compounds. Especially the high

resolution of TANSO-FTS could be beneficial for measuring these species, as is also the extended coverage towards the SWIR as compared to sounders such as IASI.

The method that we have used to measure NH_3 from GOSAT data is based on a very simple calculation that has behind it the physical principles described by the radiance of a blackbody. The method that was followed to identify ammonia can be exemplified in the following block diagram.

Fig. 28 - Block diagram.

After having downloaded the GOSAT data (Level 1B calibrated radiances) for a specific period of time and location, we have developed a routine that loads and reads the information that is contained in every file, corresponding to a single recorded spectrum. That information can be divided in four different groups, each one corresponding to a spectral band – visible, shortwave infrared and thermal infrared. For this work, we have only used the information contained in the thermal infrared range, which corresponds to the band number four. The method is, however, applicable to the SWIR, using the NH_3 signature in the band 3.

For the calculation of the brightness temperature, the radiance values and wave numbers are required, according with the equation (3.15). Inside a loop, this calculation is done for all the GOSAT spectra that were downloaded. Brightness temperature is computed for three different wave numbers, one that is sensible to ammonia and the other two that are in absorption-free regions. We are informed on the presence of ammonia in the spectrum when the brightness temperature difference between the sensitive channel (target channel) and two the window channels (baseline channels) exceeds the value of noise. The value of noise is estimated from the spectrum in an absorption free window to be ~0.15 K (2σ), peak to peak.

$$\Delta BT = BT(\text{baseline}) - BT(\text{target}) \tag{4.1}$$

$$\Delta BT = \left[\frac{BT(\text{channel 1}) + BT(\text{channel 2})}{2}\right] - BT(\text{target}) \tag{4.2}$$

Note that the channels are chosen to follow the method used to measure NH_3 with IASI in the ν_2 vibrational mode band around 950 cm^{-1} (table 9). These channels are listed in table 10.

Table 9 - Vibration modes for NH_3; source: HITRAN website.

Mode	Wave number [cm^{-1}]	Description
ν_1	3337	Stretch
ν_2	950	Deformation
ν_3	3444	Stretch
ν_4	1627	Deformation

Table 10 – Channels used to calculate the brightness temperature difference with TANSO-FTS and IASI.

	Channel 1 [cm^{-1}]	Channel 2 [cm^{-1}]	Target channel [cm^{-1}]
GOSAT	952,20	975,46	967,31
IASI	952,25	975,50	967,25

Except in some rare situations (temperature inversion in the lowest layers of the atmosphere), the emission by the Earth surface is attenuated by the atmospheric gases and, provided NH_3 contributes to the attenuation, we anticipate to calculate positive values of the brightness temperature differences following equation (4.2). Furthermore, the more positive the value, the strongest the strength of the NH_3 feature in the spectrum.

After this calculation is done, the results can be plotted in function latitude and longitude. Doing so for the three days of GOSAT allows a global view of the distribution of NH_3. Again only those values of brightness temperature that are above the noise can be unambiguously assigned to the ammonia signature.

4.3.3. Global NH_3 and comparison with IASI

In order to see how ammonia is distributed globally and how GOSAT can view that very same distribution, we have analyzed three days during the month of March 2010 providing a quasi-global coverage of the Earth surface.

This way, after applying the method described in the previous section, the results were plotted in a global map as shown in figure 29, where the color scale represents the brightness temperature difference values.

First observation to make from figure 29 is regarding the empty spaces seen in the plot. Even though we collected three days of data, proving some overlaps at high latitudes, this is not the case at tropical and mid-latitudes. The important conclusion, however, is that it is possible to identify some regions with enhanced ammonia, such as above North America, Africa, India and around the region of Thailand (flagged with a red ring). Brightness temperature differences well above 2 K are observed in these regions, which is one order of magnitude larger than the noise value (~ 0.15 K). Due to the gaps in the data it is difficult to know what the extension is of these areas where ammonia was identified.

A third observation relates to the fact that all the flagged areas where GOSAT could identify ammonia, belong to the northern hemisphere. A last observation can be made regarding the fact that the four flagged areas are all of them above land, suggesting that only the emission hotspots are detected and that NH_3 is not transported far away from the sources. This is consistent with the short lifetime of that specie.

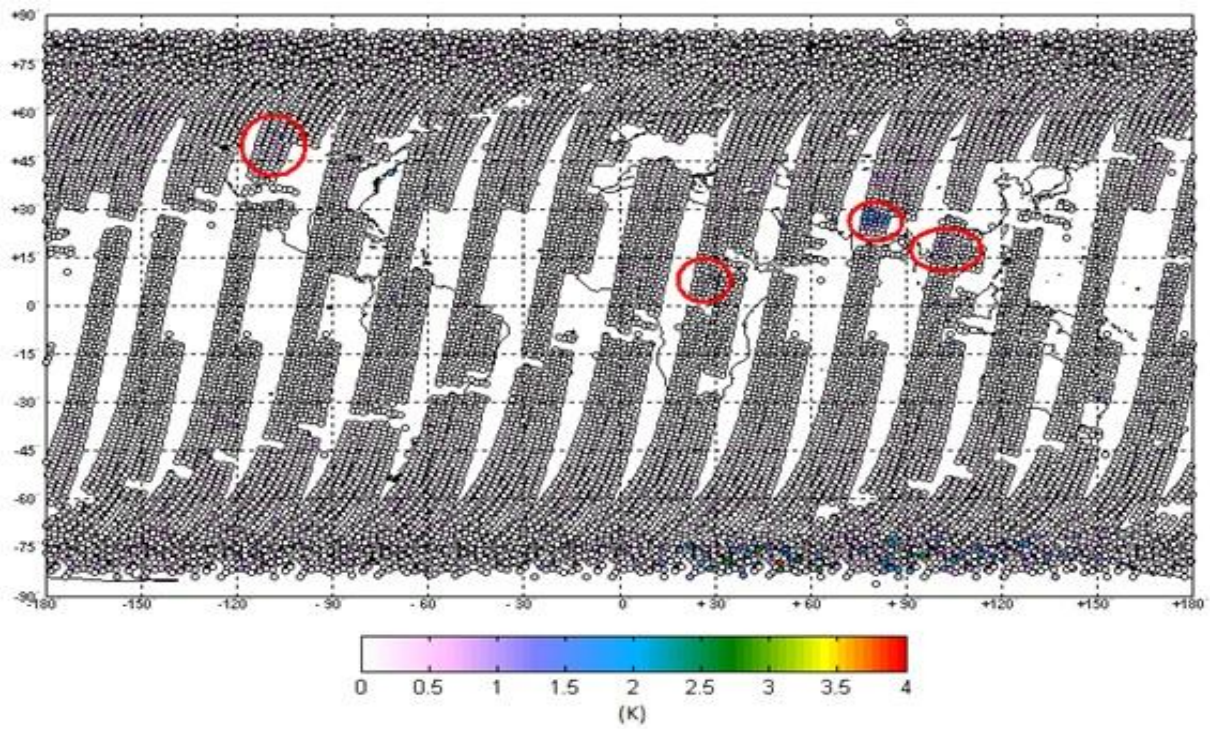

Fig. 29 - NH3 distribution obtained by TANSO-FTS in 3 days (12th, 13th and 14th of March 2010).

The same procedure was made for data recorded by IASI, during the same period of time so that we were able to compare the results obtained by both. The global map shown in figure 29 represents the global distribution of ammonia calculated in brightness temperature difference.

Contrary to what was said about GOSAT, with three days of IASI data we could have a full global coverage, and this way we do not observe any empty spaces in the map as seen for GOSAT.

The values of the brightness temperature differences with IASI are mostly around 0.3 K or below, while the IASI noise is around 0.15-0.2 K. This explains the noisy character of the distribution. Comparing figures 29 and 30 suggest a higher sensitivity of GOSAT to NH_3 as compared with IASI, at least on these 3 days basis. This is can be explained by the better spectral resolution of TANSO-FTS over IASI and the increase of line strength that follows. Although less sensitive, IASI has the advantage over TANSO-FTS of spatial sampling and coverage. Averaging IASI measurements over a month or more removes the noisy character of the distributions and enables to well identify the world's ammonia hotspots (Clarisse, Clerbaux, Dentener, Hurtmans, & Coheur, 2009).

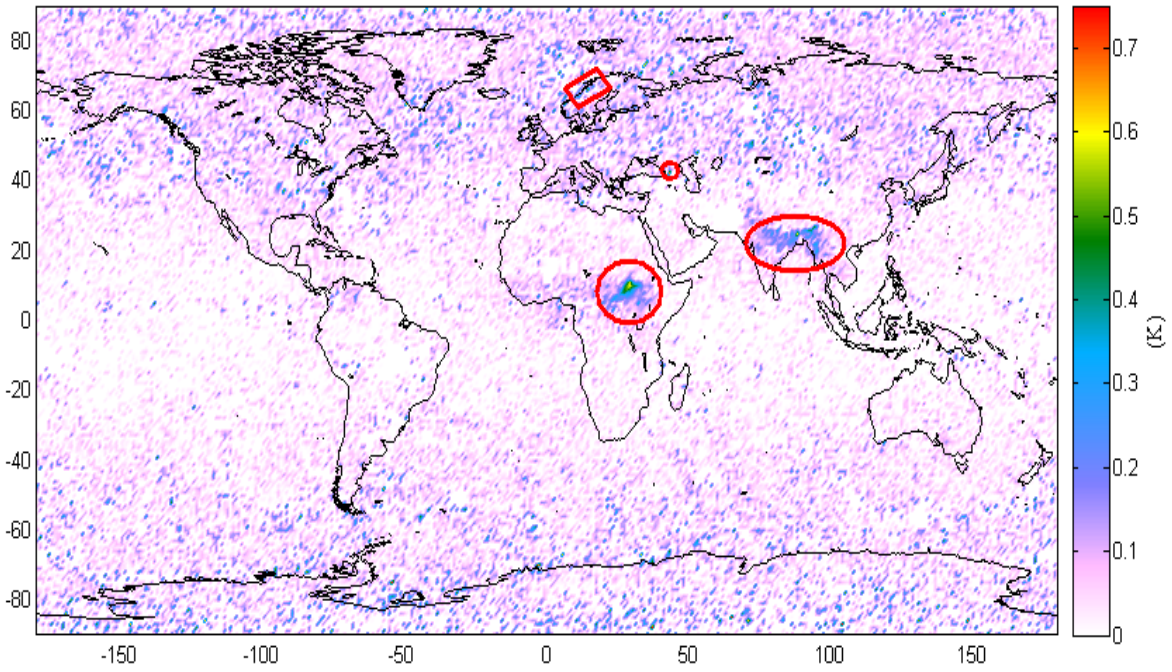

Fig. 30 - NH_3 global distribution obtained by IASI (12th, 13th and 14th of March 2010).

4.3.4. NH_3 above India: seasonal variations and comparison with IASI

In this section, we examine if there is a seasonal variation of the concentration of ammonia and if both satellites can monitor it or not. For this purpose, spectra from April 2009, July 2009, October 2009 and January 2010 were analyzed above one of the principal hotspot region (Northern India) in order to represent each of the seasons. The results obtained for spectra recorded by IASI are presented in figure 31.

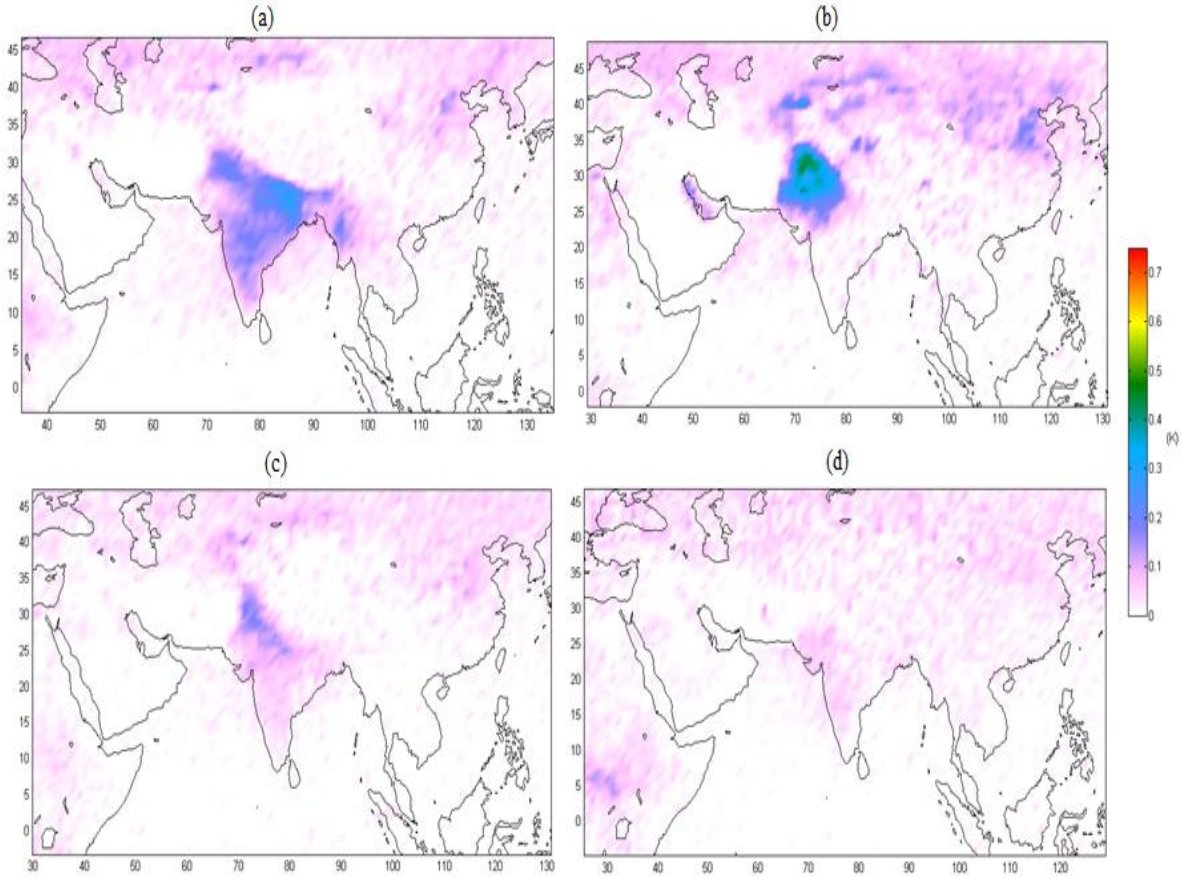

Fig. 31 - NH_3 seasonal variation obtained by IASI: (a) April 2009, (b) July 2009, (c) October 2009, (d) January 2010.

Since there is a direct link between brightness temperature differences and the concentration, it is easy to detect a seasonal variation for ammonia without having to perform sophisticated retrievals. From figure 31 we see that the concentration of ammonia is greater during April and tends to decrease along July and October, while in January there was no record of the presence of ammonia in the IASI spectra above that area. These seasonal patterns are similar to those reported for the year 2008 (Clarisse, Clerbaux, Dentener, Hurtmans, & Coheur, 2009).

The same procedure was made for GOSAT data, but for July 2009, October 2009, January 2010 and April 2010. The use of April 2010 is made because of the unavailability of the data for 2009.

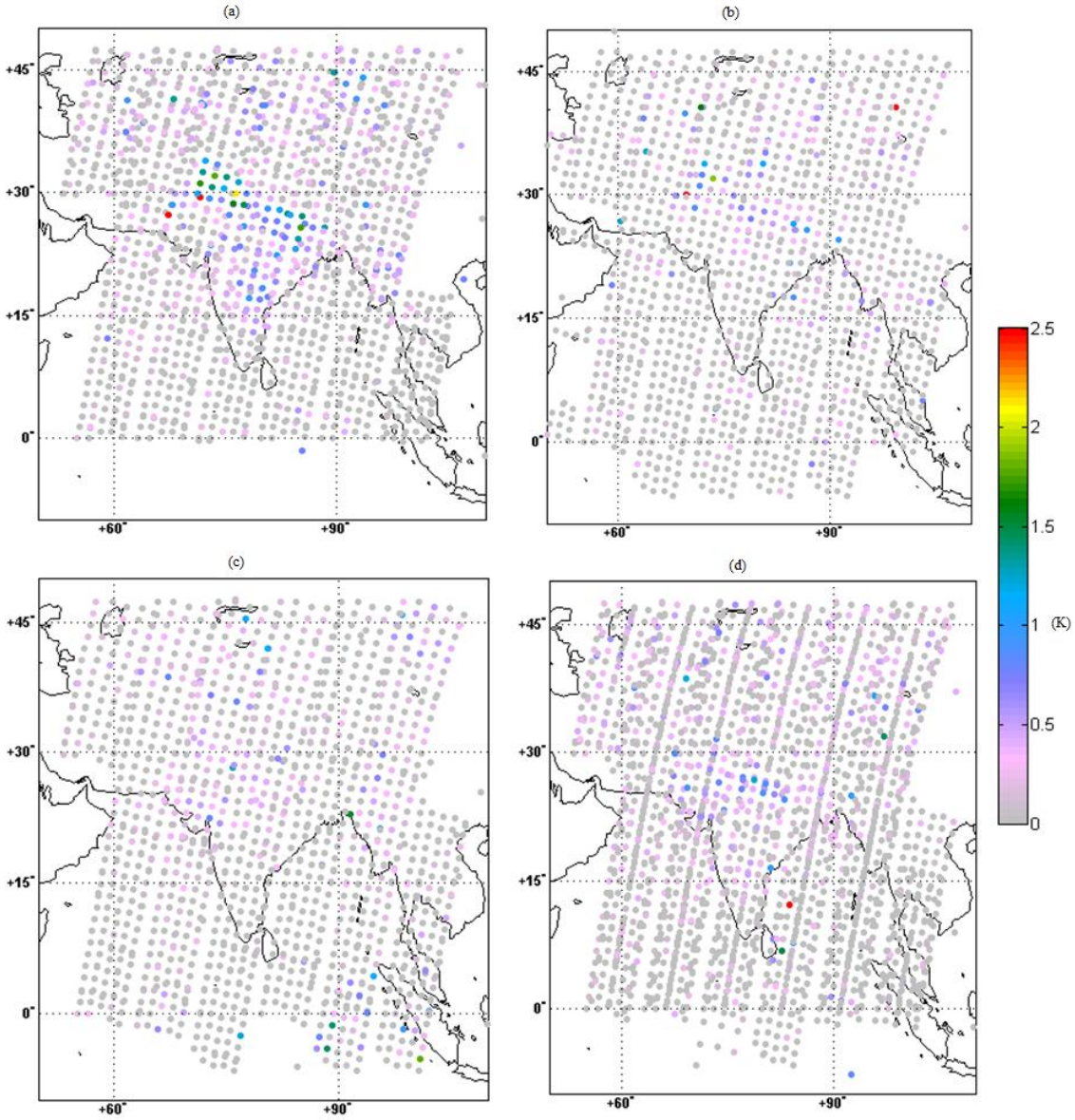

Fig. 32 - NH_3 seasonal variation obtained by GOSAT: (a) April 2010, (b) July 2009, (c) October 2009, (d) January 2010.

Figure 32 shows the results obtained for the TANSO-FTS. These results show that during the months of April and July the concentration of NH_3 is higher than during October and January. April was the month where NH_3 was more visible followed by July. These results are in agreement with the ones that were obtained by IASI (figure 31). However, as for the three days distributions it seems that ammonia is better detectable with TANSO-FTS. The presence of NH_3 in January is for example seen in the dataset while it was not the case with IASI, possibly because of a lower sensibility threshold.

Chapter 5

Conclusions and perspectives

In this work we have performed a set of first analyses of the atmospheric spectra recorded by the TANSO Fourier Transform spectrometer onboard GOSAT satellite. GOSAT is dedicated to monitoring the atmospheric abundances of CO_2 and CH_4 with unprecedented accuracy, with the objective to improve on the determination of the surface fluxes of these two major greenhouse gases and hence to contribute to climate monitoring. To achieve its science goals, the TANSO-FTS was designed with a series of key attributes for sensing the atmospheric composition in comparison to other satellite sounders: It covers a broad spectral range of the thermal infrared (from 550 to 1800 cm^{-1}), has two spectral bands in the shortwave infrared (4800-5200 and 5800-6400 cm^{-1}) and one additional visible band (12900-13200 cm^{-1}), all measured with a high spectral resolution of 0.2 cm^{-1}. Altogether, these specifications are such that TANSO-FTS could be useful to atmospheric chemistry issues in addition to contributing to climate monitoring.

In a first part of our work, we have performed a series of forward simulations in the different spectral regions covered by TANSO-FTS to confirm this, by identifying species that are potentially detectable in the measurements, besides CO_2 and CH_4, which are the obvious targets. Our analyses have revealed in particular that some of the nitrogen compounds could be measurable by TANSO-GOSAT: the thermal infrared band includes indeed absorption of N_2O, HNO_3 an NH_3, also used by other sounders (including IASI) while band SWIR 3 has also absorption band of NH_3 and N_2O. In addition, C_2H_2 and HCl were shown to absorb weakly in band SWIR 2. Interestingly, one prominent spectral band in the short-wave infrared around 6300 cm^{-1} could not be identified.

Although it has not been possible in this work to fully gauge the usefulness of TANSO-FTS to monitor reactive nitrogen compounds –in particular no retrieval and no error analyses have been performed–, we believe there are some promises in the measurements because of the high spectral resolution in the thermal infrared and because of the SWIR channels, which should both be highly favorable for probing the compounds down to the surface, where the emission

spots are. Future work should for instance study the SWIR spectra above well-known ammonia hotspots to see whether the weaker signature of ammonia in that region can be exploited or not.

In a second part of our work, we have analyzed more in depth the thermal infrared measurements of TANSO-FTS in parallel to the measurements of the IASI sounder on MetOP, which have been carefully examined and validated in the last years. First we have performed an intercomparison between IASI and GOSAT radiances, over a restricted area of the South Pacific Ocean, but with relatively stringent criteria of spatial and temporal matching and found out that the TANSO-FTS radiance measurements were biased high by about 2K for day-time measurements (note that IASI was shown not to suffer any significant bias in comparison to other sounders), even after strict removal of all scenes possibly affected by low clouds. This is an important result that will need to be addressed as a 2K error may lead to inaccurate retrieval of trace gas abundances, especially in the boundary layer. For night-time measurements, the bias is about -0.7K which is not as significant. In the same way, we also came to the conclusion that the theoretical TANSO-FTS instrument line shape was not perfectly adapted for modeling the spectra in the thermal infrared, which is another limiting factor for performing complete radiative transfer and retrievals.

For the above reason, we have decided to work on the measurement themselves, without carrying out radiative transfer simulations, and to focus in particular on the ammonia signatures around 967 cm^{-1}. We have developed a radiance indexing method similar to IASI but adapted for the TANSO spectral resolution and sampling, to robustly identify the presence of NH_3 in the spectra based on a brightness temperature difference calculation. This method was applied on 3 full days of TANSO-FTS observations to draw a first quasi-global distribution of that species. A series of hotspots have been identified, in good qualitative agreement with IASI. Above the major hotspot (Northern India), however, brightness temperature differences around 2 K were measured, far larger than the estimated noise of 0.2 K. When compared to the results obtained from IASI, i.e. brightness temperature differences of 0.3 K over a noise of 0.2 K, this suggests a much improved sensitivity threshold of the TANSO-FTS in comparison to IASI. Similar conclusions are drawn by analyzing the seasonal variations of the signal above Northern India: the seasonal patterns are agreeing but with TANSO-FTS providing better sensitivity and enabling, for instance to measure NH_3 also during wintertime when the concentrations are expected to be less. These are important results, which open promising perspectives for probing NH_3 with TANSO-FTS, to complete the picture obtained with the much larger IASI dataset. One particular aspect which could be exploited is the time difference between IASI and TANSO-FTS (about 3 hours), to try to extract information on the diurnal variations of the NH_3 concentrations.

Chapter 6

References

Andrews, D. G. (2000). *An Introduction to Atmospheric Physics.* Cambridge University Press.

Atmosphit. (n.d.). Retrieved from Galaxian Programming Consortium: http://home.scarlet.be/dhurtma/atmosphit.html

Burkhardt, J., Sutton, M. A., Milford, C., Storenton-West, R. L., & Fowler, D. (1998). Ammonia Concentrations at a site in southern Scotland from 2 yr of continuous measurements. *Atmospheric Environment* , 325-331.

Clarisse, L. (2010). Retrieving ratios, concentrarion, optical depth and mass of different types of aerosols from high-resolution infrared nadir spectra., (p. 49(21)).

Clarisse, L., Clerbaux, C., Dentener, F., Hurtmans, D., & Coheur, P.-F. (2009). Global ammonia distribution derived from infrared satellite observations. *nature geoscience* .

Clerbaux, C. (2009). Monitoring of atmospheric composition using the thermal infrared IASI/MetOp sounder. *Atmospheric Chemistry and Physics* .

Coheur, P.-F., Clerbaux, C., Clarisse, L., Dentener, F., Martin, R., Sutton, M., et al. (n.d.). NITROSAT The first mission dedicated to monitoring of reactive nitrogen.

Galloway, J. N., & Aber, J. D. (2003). The Nitrogen Cascade. *BioScience* , 341-356.

GOSAT. (2009). TANSO onboard GOSAT Appendix A - Outlines of GOSAT and TANSO sensor.

Gupta, A., Kumar, R., Kumari, K. M., & Srivastava, S. S. (2003). Measures of NO_2, HNO_3, NH_3 and SO_2 and related particular matter at a rural site in Rampur, India. *Atmospheric Environmental* , 4837-4846.

Hamazaki, T., Kaneko, Y., & Kuze, A. (n.d.). Carbon Dioxide Monitoriong from the GOSAT satellite.

Hatch, D. J., & Jarvis, S. C. (1990). Measurements of ammonia emission from grazed grassland. *Environmental Pollution* , 333-346.

Hurtmans, D. (1995). *Measures d'intensités spectrales absolutes par spectrométrie Fourier dans le domaine infrarouge appliquées à des molécules d'intérêt atmospherique, PhD Thesis.* Brussels: Université Libre de Bruxelles.

Illigworth, S. M., Remedios, J. J., & Parker, R. J. (2009). Intercomparison of integrated IASI and AATSR calibrated radiances at 11 an 12µm. *Atmospheric Chemistry and Physics* , 6677-6683.

Kasper, A., & Puxabaum, H. (1998). Seasonal variations of SO_2, HNO_3, NH_3 and selected aerosol components at Sonnblick (3106 m a.s.l.). *Atmospheric Environment* , 3925-3939.

Kuze, A., & Suto, H. (2008). *TOKYO and TSUKUBA Models - Tanso Precursor Experiments.* Japan: Japan Aerospace Exploration Agency.

Petty, G. W. (2006). A first course in atmospheric radiation - 2nd edition. *Sundog Publishing* .

Svensmark, H., & Friis-Christensen, E. (1997). Variations of cosmic ray flux and global cloud coverage - a missing link in solar-climate relationships. (pp. 1225-1232). Journal of Atmospheric and Solar-Terrestrial Physics.

The HITRAN database. (n.d.). Retrieved from http://www.cfa.harvard.edu/hitran/

Wespes, C. (2010). *Measures de l'acide nitrique dans l'atmosphère à partir d'observations satellitaires dans l'infrarouge thermique, PhD thesis.* Brussels: Université Libre de Bruxelles.

Yasuoka, Y. (2010, January). NIES GOSAT Project Newsletter #1.

Yokota, T., Yoshida, Y., Eguchi, N., Ota, T., Tanaka, T., Watanabe, H., et al. (2009). Global concentrations of CO2 and CH4 retrived from GOSAT: First Preliminary Results. *SOLA* , 160-163.